A Planning Tool for Left Ventricular Reconstruction in Patients with Severe Ischemic Cardiomyopathy

Praneeta R. Konduri

Technische Universiteit Delft

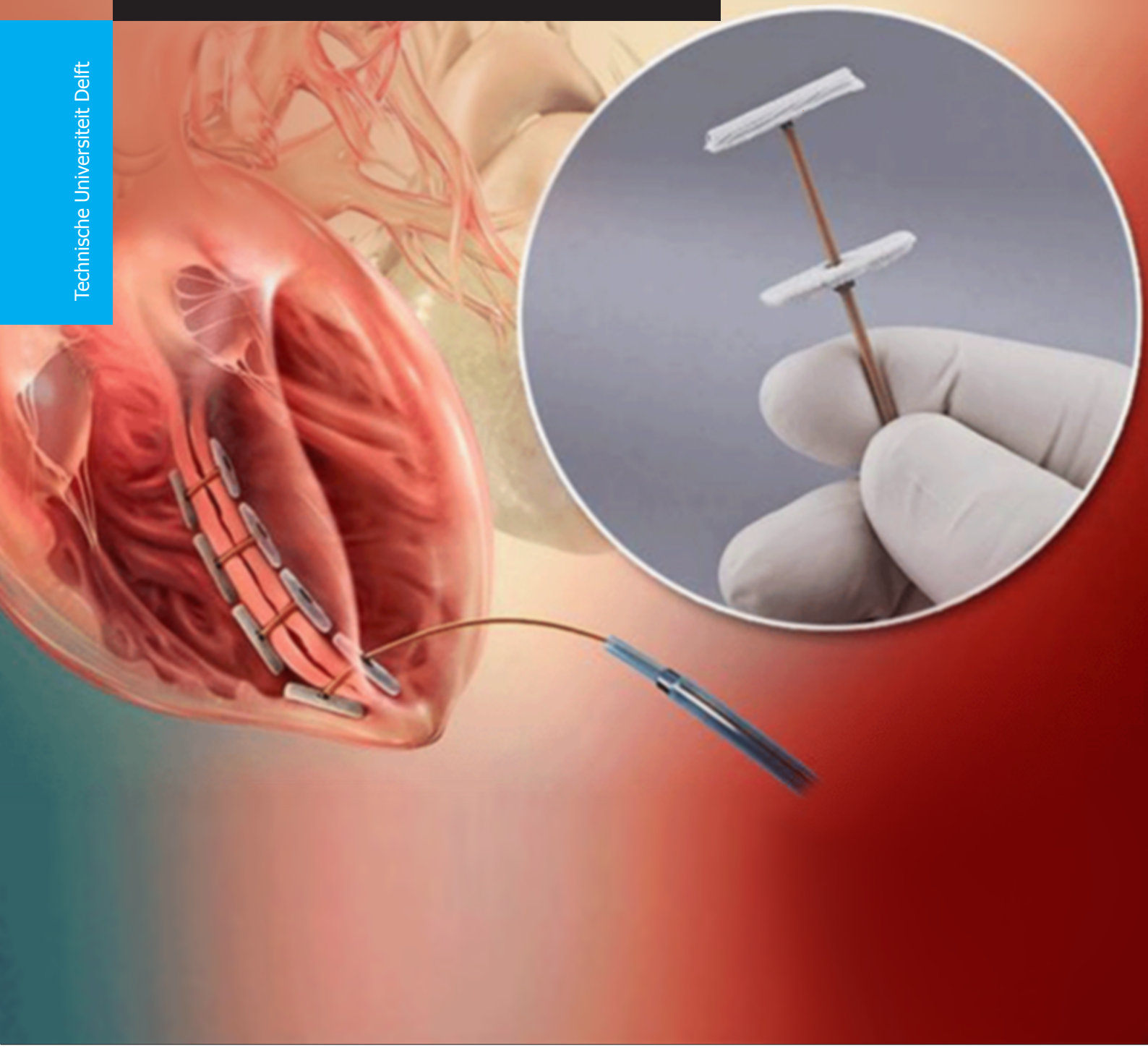

TU Delft Delft University of Technology

Challenge the future

A Planning Tool for Left Ventricular Reconstruction in Patients with Severe Ischemic Cardiomyopathy

by

Praneeta R. Konduri

in partial fulfillment of the requirements for the degree of

Master of Science
in Biomedical Engineering

at the Delft University of Technology,
to be defended publicly on Wednesday August 16, 2017 at 10:00 AM.

Supervisor:	dr. H. A. Marquering,	Academic Medical Center
	dr. F. M. Vos,	TU Delft
Thesis committee:	dr. F. M. Vos,	TU Delft
	Prof. dr. J. Dankelman,	TU Delft
	Ms. N. Sarkalkan,	TU Delft
	dr. H. A. Marquering,	Academic Medical Center

An electronic version of this thesis is available at http://repository.tudelft.nl/.

TU Delft Delft University of Technology

Preface

I want to thank Dr. H.A. Marquering for giving me the opportunity to be a part of this project and to work at the Department of Biomedical Engineering and Physics at the Academic Medical Centre, Amsterdam. I express my deepest gratitude to him, for always taking time out to guide and encourage me. Furthermore, I would like to thank Dr. Frans Vos for accepting to supervise this project and for his technical insights. I want to thank Dr. R. N. Planken and Dr. W. J. P van Boven for providing the required clinical inputs. I am also grateful to Merel Boers, Dr. Emilie Santos and Manon Tolhuisen for their continued assistance during the course of this thesis.

Praneeta R. Konduri
Delft, August 2017

Abstract

Background and purpose: The Revivent Myocardial Anchoring System (RMAS) is a surgical ventricular reconstruction technique that plicates the scarred region with anchors to achieve at least 30% reduction in the Left Ventricular (LV) volume and at most 40% occlusion of the Right Ventricular Outflow Tract (RVOT) by the plicated region. As this is a minimally invasive procedure, the surgeons need to rely on pre-surgical imaging rather than peri-procedural visuals to plan the location of the anchors. This study presents an *in-silico* modelling tool to estimate the effect of this reconstruction procedure on the function and geometry of the residual LV.
Methods: The planning tool developed in this study is based on pre-operative (mainly cine Cardiac MR) imaging from which the LV contours are extracted. The proposed solution corrects for slice misalignment due to breathing motion and patient movement during image acquisition. The extent and the location of the scar are identified on contrast enhanced Cardiac MR images and used to classify the LV short axis contour points into scarred and healthy segments. The surgery is simulated by reconstructing each residual LV short axis contour as a circle obtained from the healthy segment. The simulated residual LV volumes at end-diastolic and end-systolic phase, stroke volume, and ejection fraction are compared with the baseline characteristics. Occlusion of the RVOT by the plicated scar is quantified. The shape of the residual LV is also compared with that of two geometrical models using a shape descriptor called curvedness as a parameter.
Results: The *in-silico* analysis was performed for all four patients who have been treated or considered to be treated with the RMAS at the AMC. Visual analysis of the images corrected for breathing motion and patient movement showed a smoother transition of the LV between short axis image slices compared to the original image stack. Volume reduction of the *in-silico* analysis in the range of 34 – 55% at end-systolic phase and 29-51% at the end-diastolic phase was observed. An improvement of ejection fraction in the range of 12-96% was also observed. The required functional end-points are met for all four patients.
Conclusion: The presented approach allows the surgeon to simulate different LV residual models by changing the location of the anchors. This tool shows promising results but needs to be validated by comparing using a larger database with post-surgical scans to determine the accuracy of the *in-silico* method and to obtain a more comprehensive understanding of the surgery.

Keywords: Surgical ventricular reconstruction, Planning tool, Ischemic Cardiomyopathy

Contents

1 Introduction

1.1. Ischemic Cardiomyopathy

Ischemic Cardiomyopathy (ICM) is a disease that affects the myocardium and is caused by narrowing of the coronary arteries leading to a decrease in the supply of oxygen to the myocardium [1]. According to the World Health Organisation, ICM is the most common cause of death globally. Heart failure in the developed world is mostly caused due to ICM [2]. Treatment of acute myocardial infarction through techniques like thromolytic and percutaneous coronary intervention have been successful in improving patient survival. But, these techniques can cause Left Ventricular (LV) remodelling and chronic myocardial dysfunction, thus, increasing morbidity. According to [2], ICM is defined as "LV systolic dysfunction with one or more of the following: a history of prior myocardial revascularisation or myocardial infarction, more than 75% stenosis in the left main stem or left anterior descending artery, or two vessels or more with a greater than 75% stenosis".
ICM consists of a spectrum of differing physiological, molecular and structural changes ranging from myocardial stunning, hibernation and myocardial scarring [2]. Myocardial stunning refers to a state of persistent reversible hypo-contractility even after blood flow has been restored following transient or recurrent ischemia. Hibernation also presents similar physiological changes that are followed by structural changes at the cellular level. Chronic hibernation can lead to an increase in the extra-cellular space and fibrosis development, resulting in scarring. The three phases of this spectrum will lead to LV remodelling, which can occur at any stage of the spectrum. LV remodelling that occurs in the early stages consists of dilation and wall thinning, while, the later stages lead to irreversible geometric and functional changes [2].

1.2. Management of Ischemic Cardiomyopathy

The management of ICM involves differentiating patients with hibernating myocardium from the patients that have scarring and related irreversible remodelling. Imaging modalities like Echocardiography, Nuclear Imaging, Computed Tomography and Cardiac Magnetic Resonance are used to identify the viable myocardium i.e, the region of the myocardium that consists of cells that are alive and upon restoring the metabolic activity of the membrane, can become contractile due to their reserve contractile function. Myocardial viability is often used as a predictor of revascularisation therapies aimed to restore LV function. The physics governing the different modalities is closely related to the functional assessment provided by that modality [2]. This section briefly describes the role of Cardiac Magnetic Resonance in the management of ICM.

Cardiac Magnetic Resonance (Cardiac MR)

Cardiac MR can help to obtain information about the underlying etiology and to identify viable, at-risk and ischemic regions of the myocardium. A prior infarction, especially in the coronary arteries can lead to abnormal wall motion and regions of akinesis, which can be identified through Cardiac MR. Thinning of myocardium in cine Steady State Free Precision images is used to detect akinetic regions (Figure 1.1(a)). Administering gadolinium contrast helps to locate regions of myocardial fibrosis

as the gadolinium contrast accumulates in regions of expanded interstitial space (fibrotic or scarred regions). This accumulation increases the T1 signal intensity in inversion recovery T1 weighted signals. The pattern of high intensity regions can distinguish the underlying etiology. For example, ICM is characterised by a transmural scar, where the extent of transmurality is correlated with the severity of the condition. On the other hand, non-ischemic cardiomyopathy is generally characterised by diffuse or patchy scarring not corresponding to a coronary artery. The extent of scarring is used as a marker to predict recovery in contractile function after revascularisation. Late Gadolinium Enhancement less than 25% is considered as viable, 25-75% as intermediate and above 75% as nonviable. T2 weighted images are used to recognise areas of risk as the high signal areas are larger than in the corresponding Late Gadolinium Enhancement images, indicating regions that can regain their contractility function after revascularisation. However, reproducibility is a disadvantage of this method owing to high signal artefacts by the high signal from blood flow and field inhomgeneities [3]. Cardiac MR offers flexibility

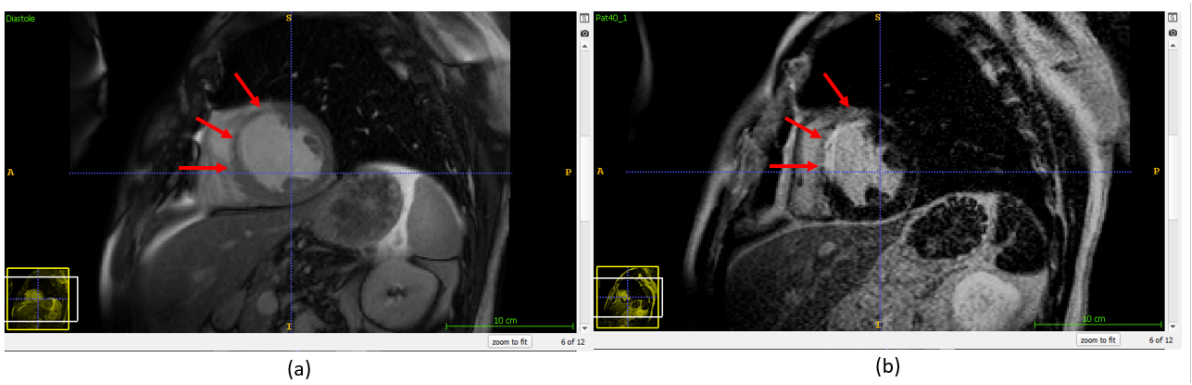

(a) (b)

Figure 1.1: (a) Cine SSFP image of a slice at systole. Thinning of the myocardium is indicated by the arrows. (b) Delayed Hyper-Enhancement (DHE) Cardiac MR of the same slice with the corresponding transumral scar pointed by the arrows

.

to image the heart in any plane without being limited by a window as in the case of echocardiography. This allows for functional information to be assessed with higher accuracy and reproducibility without geometrical assumptions. Improving imaging techniques to speed up the acquisition may increase the popularity of Cardiac MR to make it available for routine assessment of patients [3].

1.3. Treatment

Treatment options for ICM include heart failure medications, revascularisation therapies through angioplasties or bypass surgeries and cardiac or left ventricle assist devices and transplantation. Patients with ICM due to myocardial infarction undergo a remodelling process that causes dilation of the LV leading to an increase in its volume and a decreased contractile function. The prognosis decreases as the remodelling increases leading to a more spherical LV shape. Such patients are treated with surgical therapies. Coronary Artery Bypass Graft is the most basic treatment technique, however, it cannot produce sufficient improvement in the LV function as the remodelling process continues despite the revascularisation of the ischemic area [4].
Surgical Ventricular Reconstruction (SVR) has been introduced to treat patients with severe ICM and it aims to restore the effects of LV remodelling in terms of shape, size and function by reducing the LV wall stress. According to Laplace's Law, LV wall stress is directly proportional to the LV radius and pressure while being inversely proportional to LV wall thickness. Under cardioplegia, an opening is introduced in the center of the scarred region after performing other surgical procedures when required. The non-contractile myocardial regions are excluded by placing a Dacron patch at the junction of the healthy endocardial muscle and scarred myocardium. A balloon or a mannequin of appropriate volume and geometry is introduced into the LV to ensure that residual volume of the cavity is sufficient. The balloon or the mannequin is removed before closing the LV (Figure 1.2). In cases of extreme apical dilation, the distal inferior wall is plicated before placing the Dacron patch. Myocardial revasclarisation of the proximal Left Anterior Descending artery is performed along with mitral valve repair when required [5].

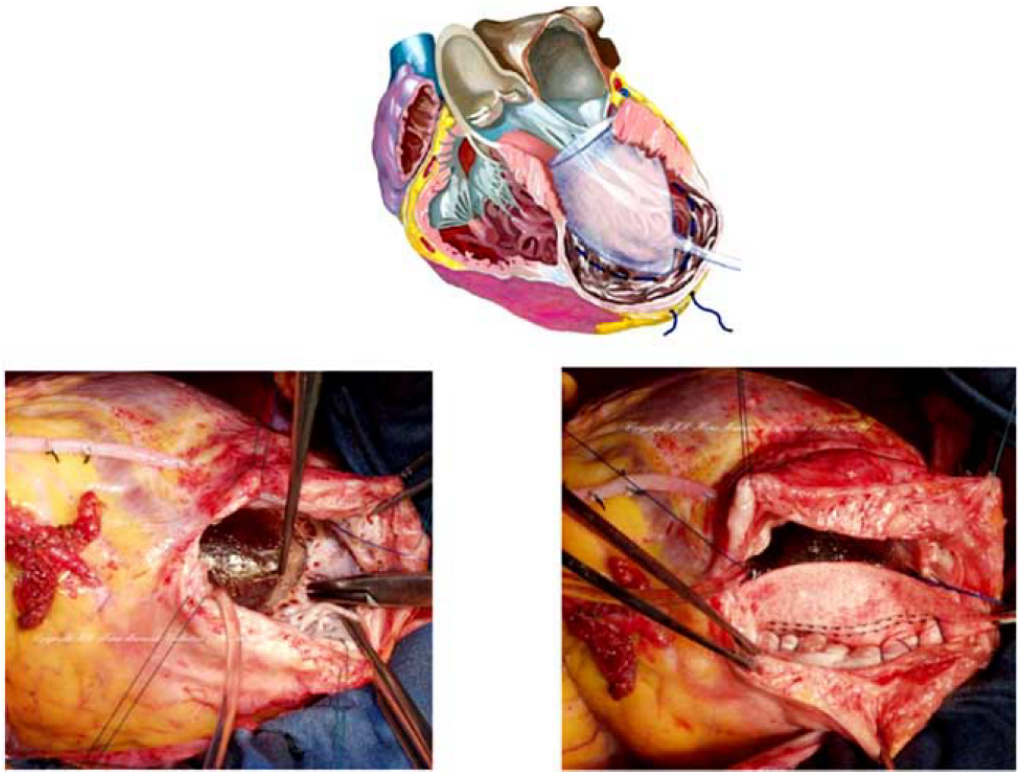

Figure 1.2: *Top*: Schematic representation of a mannequin used in SVR *Bottom*: The mannequin is used to guide the reshaping of the ventricle to achieve the required elliptical shape (*left*) and the Dacron patch closes the opening in the LV (*right*) [5]

.

1.3.1. Revivent Myocardial Anchoring System

Revivent Myocardial Anchoring System (RMAS) (Bioventrix Inc., San Ramon, CA) has developed a technique called Less Invasive Ventricular Enhancement that aims to achieve similar LV configuration as obtained from the SVR techniques but, without the incision of the LV and the requirement of cardiopulmonary bypass. The four components of the Myocardial Anchoring System are - a catheter-based delivery system, pairs of titanium anchors coated with polyester fabric, a retrieval system and a force gauge. The scarred myocardial region is plicated and excluded by the anchors - one of the anchors passes through the septum to its right side and the other anchor secures the LV epicardial position [6]. A schematic representation is shown in Figure 1.3 and Figure 1.4 shows a slice of the post operative CT scan indicating the anchors that plicate the apical region and the maximal intensity projection of the 3-D volume.

Insight from other studies

This section presents the methods used for analysing the cardiac function at baseline, selecting the locations for anchor placement and results of other studies based on RMAS. Cine Steady State Free Precision or Transthoracic Echocardiography (along with Simpson's method) has been used to estimate LV End Diastolic Volume and Ejection Fraction. In one study, TEE is used to identify the aneurysm in the anterior part of the apex, which is then verified through cardiac CT [6]. Late gadolinium enhancement is used to locate the transmural scar, which in one study, also identified an apical thrombus.
Direct Fluroscopic and/or Trans-esophageal echocardiography are used to guide the placement of the anchors. Seven anchors are required to completely plicate the scar in one study that is conducted on one subject [6]. Post-mortem studies of ovine models conducted by one group observed erosion of the anchors in the myocardium. In order to securely place the anchors, the use of a compressive force of 4N is suggested [7].
In the study conducted on one subject, an improvement in the New York Heart Association Class, significant volume reduction and improvement in ejection fraction is observed. No leakage is recorded

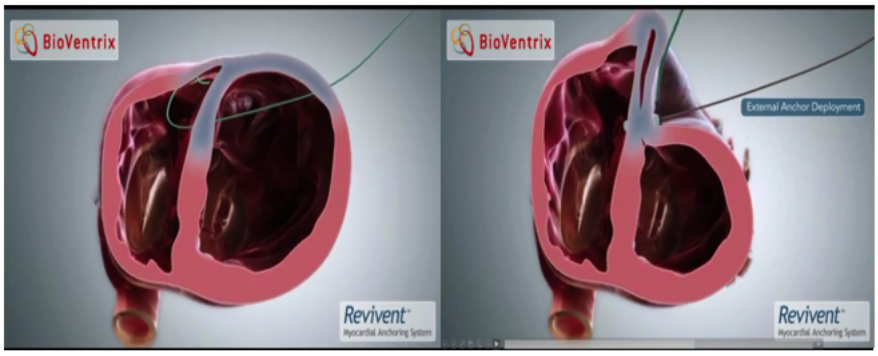

Figure 1.3: Schematic representation of the Less Invasive Ventricular Enhancement Technique [6]

.

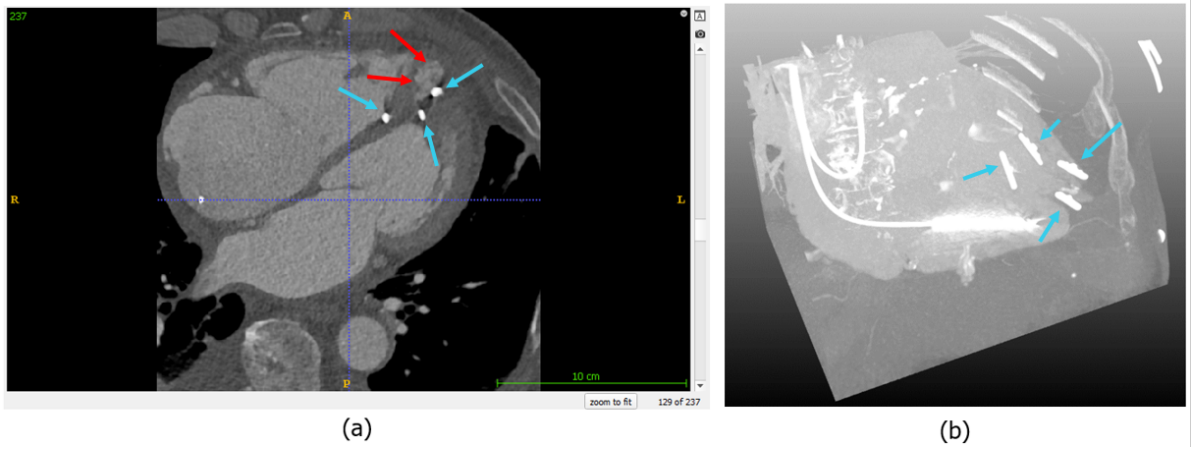

Figure 1.4: (a) A slice of the post operative scan and (b) Maximum Intensity Projection (MIP) of the 3-D cardiac volume. The blue arrows point to the anchors that are used to plicate the scarred myocardium (pointed by the red arrows)

between the healthy myocardium and the excluded scarred region right after the surgery, however, some leakage is present at the 6-month follow up. Leakage causes a risk of clots [6]. Another study, considering the results of 11 patients reported a significant decrease in End Systolic Volume and End Diastolic Volume. The volumes remained constant 6 and 12 months after the procedure, suggesting that there is no erosion in the anchors. The volume reduction obtained with this technique is comparable to other LV restoration techniques and exceeds the results obtained in the STITCH trial [7].

Due to the minimally invasive nature of the RMAS technique, surgical planning depends on the pre-procedural imaging ratehr than on the peri-procedural imaging. There is a clinical need for *in silico* modelling to estimate the effect of the surgery on the LV geometry and function. Virtual modelling of the surgery can be used as a tool to quantify the scarred regions. Such an approach can be potentially used to understand the effect of the position of the anchors on the residual cavity's geometry and function [8] so as to accurately estimate the optimal LV reconstruction.

1.4. Aim of the Project

The aim of the project is to develop an *in-silico* modelling tool that aids in the planning of surgical ventricular reconstruction through Revivent Myocardial Anchoring System by simulating the effect of the surgery and analysing the geometry and function of the residual left ventricle.

2

Literature Review

Analysing the effect of surgical ventricular reconstruction consists of quantifying the residual left ventricular geometry and function. This can be performed by comparing the left ventricular characteristics either with baseline characteristics and/or with an ideal left ventricular model. This review stems from the requirement to identify parameters or constraints that are used to describe left ventricular geometry and function. This review consists of descriptors used in left ventricular analysis and the methods used to estimate them. The results of the review are categorized into pre-processing and segmentation methods, classification of cardiac parameters into traditional and non-traditional descriptors, and methods used to estimate them.

2.1. Search and Selection

A literature search was conducted in Pubmed with the following search query:

```
(((cardiac & morphology) & (modelling | remodelling)) OR (geometric &
(modelling | remodelling)) OR (biomechanical & (modelling | remodelling)))
                        AND (magnetic & resonance)
```

The inclusion criterion are:

- Papers that developed/ described/ implemented methods to obtain descriptors of cardiac structures from anatomical MR/ CT images
- Papers that derive left ventricular functional parameters to describe LV remodeling in different pathologies

The exclusion criterion are:

- Papers describing cardiac parameters that do not assess LV geometry
- Papers describing biomechanical/electrophysiological models not derived from geometrical models or anatomical image data
- Studies that are performed on non-human data
- Unavailability of paper

The search resulted in 331 papers and the first 75 articles are studied after using "most relevant" filter. Table 2.1 shows the classification of the results.

Table 2.1: Classification of results obtained in the literature review

Papers describing methods to correct for motion artefacts from Cardiac MR images	1
Papers developing/implementing anatomical/statistical models to estimate cardiac parameters or to develop biomechanical/electrophysiological models	12
Papers describing cardiac parameters for evaluating LV remodeling	33
Papers describing use of Cardiac MR for diagnosis/management of cardiac pathologies	2
Papers excluded	27

2.2. Pre-processing and Segmentation Techniques

Cardiac MR imaging is a part of the routine assessment of cardiac function. However, it generally suffers from slice misalignment induced from breathing motion and patient movement. A Cardiac MR image dataset generally consists of three orthogonal long-axis images and also parallel short axis images. These images are acquired over multiple breathing cycles and thus, imaging at different diaphragm locations. Patient movement during the image acquisition can further lead to misalignment, thus, decreasing the accuracy of the developed model [9]. This section first describes the techniques that are used to correct for these artefacts and then describes the segmentation methods found in this literature review that are used to develop models of cardiac structures.

2.2.1. Methods to correct breathing motion artefacts in Cardiac MR images

The methods available to correct breathing motion induced artefacts can be broadly classified into image based and geometry based techniques. Image based techniques use registration techniques aimed to increase the pixel similarity between consecutive short axis slices or between short axis and long axis slices at the intersection of these slices. A method that maximises pixel similarity by comparing several cost functions is also introduced. According to [9], correcting for breathing motion artefacts based only on images may lead to inaccurate results owing to non-uniformity and heterogeneity in images and large slice spacing (typically 8mm).

Geometry based techniques are based on aligning the geometric information (generally, contours delineating the left ventricle in short and long axis slices) to correct for slice misalignment. The short-axis contours may be aligned so the centroids of each short axis plane is better aligned to the long axis planes. In [10], an energy function based on the curvature of the LV geometry is minimized. This approach is based on the assumption that LV shape is generally convex at most vertices. However, these methods may not be successful in realigning slices for cases with LV remodelling, as with patients suffering from severe ischemic cardiomyopathy. Another drawback of geometry based approach is the pre-processing step to extract contours. This can be circumvented by using semi-automatic or automatic segmentation techniques [9].

In [9], a method to correct for motion artefacts in multi-planar cine Cardiac MR images is presented. This method has three steps - contour delineation, registration and reconstruction of LV shape from corrected contours. Contours of the LV endocardium at diastole are manually delineated on all short-axis and long-axis views using `CMRtools suite`. The 2-D contours from all the views are then projected into the 3-D Patient Coordinate System which is defined by image specifications (image orientation, pixel spacing and image position). Each short axis contour is registered to the set of long axis contours and each long axis contour is registered to the set of short axis contours iteratively using generalized Iterative Closed Point Algorithm (ICP) until convergence. The realigned short axis contours are then used to reconstruct the LV shape by first interpolating between consecutive short axis slice, then, generating a tetrahedral mesh and finally segmenting a variational mesh and extracting the surface [9]. Figure 2.1 shows the surface obtained from short axis contours before and after realignment.

This method is verified by determining the intersection between the surface reconstructed from the realigned contours and the long-axis contours that are initially drawn using Hausdorff distance, Dice Similarity Coefficient and Jaccard Similarity Coefficient. An improvement in accuracy from the original LV shape, mainly according to Dice and Jaccard Similarity Coefficient is observed [9].

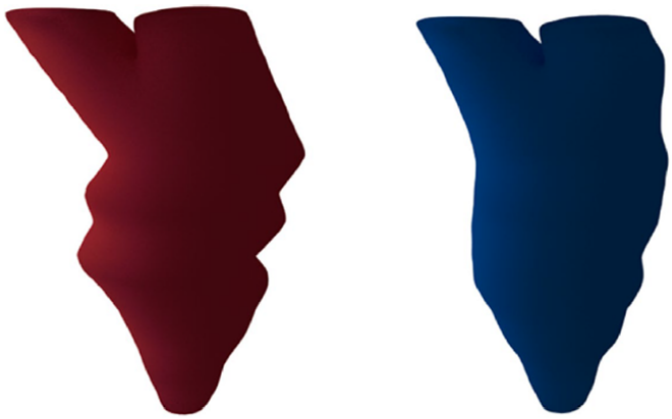

Figure 2.1: Surface reconstructed from short axis slices (a) before and (b) after realignment [9]

.

Table 2.2: List of software platforms that perform cardiac analysis found in this literature search

Software Platform	Producer	Articles
Segment	Medviso	[8][11][12]
Mass	Medis	[13][14][15][16][17][18][19]
TomTec 4D	TomTec Imagingsystems	[20][18]
Syngo	Siemens Healthcare	[21][22][23]
CMR Tools	Cardiac Imaging Solutions	[24][25]
View Forum	Philips Medical Systems	[26]
Cardio Viewer	Bio-Lynx	[27]
Argus	Siemens Healthcare	[25][28][29]
ImageJ	National Institutes of Health, USA	[30]
GE Advantage	GE Healthcare	[31]

2.2.2. Segmentation Techniques

The following section classifies the segmentation techniques found in this review into three categories - manual contour delineation, semi-automatic and automatic methods, based on the level of user input required for segmentation.

Manual contour delineation

Several software platforms are available that allow manual contour delineation for segmentation and also to perform geometrical and functional analysis of the left ventricle. The list of software found in this literature search are shown in Table 2.2.

Software based semi-automatic segmentation

1. Custom-built Software:

   `HeartGen:`

   In [32], a web service (`HeartGen`) that provides a meshing solution for cubic Legrange or cubic Hermite meshes with maximum stability and accuracy to generate personalized computational meshes of the left ventricular, right ventricular and/or bi-ventricular geometry is presented. Input to the system is a binary mask that represents the ventricular domain. The personalization of the template (truncated ellipsoids with topology and number of elements set by the user) is achieved through four steps. First, geometrical features are extracted from the binary mask and then used to initialize the template. The initial binary mask and the template are then aligned through affine registration. A user-defined parameter is introduced to address the trade-off between fitting accuracy and numerical stability. After warping the template through a variational technique, post processing to increase the quality of the mesh by modifying the derivative at each node in the radial direction so that it is forms a straight line between opposite nodes (across the

wall) is performed. This technique provides smooth meshes, even in cases with sparse data and can also be extended to extract other anatomical segments too. However, it still requires the initial shape (binary mask) and the template to be defined.

MRICad:

In [33], a computer package, `MRICad` to generate tetrahedral meshes of the thorax and the heart to solve the forward and inverse electrocardiographic problems is introduced. The resulting tetrahedral meshes for each organ can be distinguished on the basis of their properties which depend on the electrical conductivity of that organ/tissue. DICOM slices are accepted as input where the user can semi-automatically segment the various organs (and assign a tissue label from 33 pre-defined labels) using splines. A poly-line or a contour line is used to attach the new point to the previous point to obtain a segmentation. Edge detection filters are incorporated to highlight the edges. A graph map for each organ is then generated by the software. Cubic meshes are generated from these maps and used as input to `TetGen` that produces Delaunay tetrahedralization along with incorporating the electrical characteristics of the regions thus, allowing these meshes to be used for solving the forward ECG problem through Finite Element Analysis. Though this technique allows to produce accurate tetrahedral meshes for different applications, it is still time-consuming.

2. Active Shape Model:
   In [34], an active shape model of the endocardial surface is generated by computing the mean of aligned surfaces as the average of the coordinates and the result of PCA is used to determine the minimum number of nodes required to describe the variability in the data. The endocardial surface segmentations are obtained from echocardiographic data of 205 subjects using the semi-automatic segmentation software - `Tomtec`. The shape model is then applied on short axis Cardiac MR images (after correcting for mis-alignment) by initializing six points in the two and four chamber views. The shape model is optimized by deforming so that it matches the LV endocardial positions in all short axis slices simultaneously, until a stable segmentation is obtained. The results are compared with the ejection fraction and end systolic volume and end diastolic volume estimated through disc area summation method and direct volume estimation (from area of triangular patches) with the golden standard (disc area summation of the contours delineated on the SAX images). The results of the segmentation include short axis contours which can be used to calculate LV volumes and as 3D endocardial meshes which can be extended for finite element analysis or mechanical studies. Though the LV volumes obtained from the contours and the mesh are comparable with the 'gold standard', the accuracy of the volume estimation depends on the variability of the training dataset.

3. Other Software:
   Several software platforms are also available that allow semi-automatic segmentation of the cardiac segments. In [35], `Mimics` software is used to segment the aorta based on thresholding and region growing algorithms and this software also provided a platform for manual editing. In [34], `TomTec` software is used to semi-automatically segment LV endocardial surfaces from echocardiographical data and export the surface as nodes and faces. The user needs to define the nodes of the mitral valve, aortic valve and the LV apex.

Automatic segmentation

Automatic localization of the left ventricle to identify a local region of interest is an important step towards reducing the volume of interest available for the automatic segmentation of the left ventricle. The methods available for automatic localization can be broadly classified into either pattern-recognition based techniques or temporal dimension approaches. In pattern recognition based approaches, the required "donut" pattern is first modelled as a multi-dimensional vector and then as a Markov process. Manually recognized positive and negative examples are used to train the system which then classifies the image pixels into the LV boundary. The accuracy of the system then depends on the relevancy of the training examples [36].

Temporal approaches exploit the fact that the heart shows substantial motion in cine images. The variance or the harmonic images (based on Fourier Analysis) produce high intensity regions that correspond to the left and the right ventricle. A circle Hough transform is then used to localize the left

ventricle. However, the robustness of this approach is affected by the movement of RV, leading to inaccurate LV region identification. To overcome this problem, in [36], it is observed that the dominance of RV in the harmonic image increases as the harmonic order increases. In this article, the first and the fifth harmonic image are used to anisotrpically weight the circle Hough Transform. The first harmonic image has the most visible LV and thus, is weighted positively, while the higher order image has higher dominance of RV and hence, is weighted negatively. This helps to reduce the RV interruption producing a better LV localization. In most segmentation techniques, the result of localization on one slice is generally projected to the other slices. However, LV and RV are present in small regions in the basal slices and the apical slices are subject to a high variation (due to motion) [36]. In this literature search, the techniques mentioned below have been used to produce automatic segmentation results which are later used for different applications.

1. Shape-constrained Deformable Models:
   In [37], to allow Cardiac MR-guided LV lead implantation, the slowest mechanically activated regions of the healthy myocardium are identified and then combined with fluroscopy during implantation. To facilitate this process, the epicardial and endocardial surfaces of left ventricle, left atrium, right ventricle, right atrium are segmented automatically using a shape constrained deformable model. This is done with the help of a deformable mesh represented by vertices and triangles describing all required cardiac segments mentioned above. The first step is to localize the heart using 3-D Generalized Hough Transform that is applied on a thresholded edge map of the down-sampled Cardiac MR image. The images used for training are also used to obtain the R-table of Global Hough Transform, the mean mesh and to describe a boundary function for every triangle. The mesh is adapted by repeating the boundary detection step (searching for boundary points along the normal of the triangles) and by deforming the mesh so as to minimize the distance between the boundary points and the triangle centers. To constrain the deformation, the objective function is then defined to minimize energy (which is the the sum of external (distance between the target points and the triangle centres) and the weighted internal energy that is used to constrain the shape deformation). The boundary detection step and the energy minimization are iterated until a stable segmentation is obtained. This method can produce segmentations in less than a minute. Moreover, image calibration to correct for image intensity variations further decreases the segmentation errors, mainly reducing the number of triangles with medium to large errors [38].

2. Marginal Space Learning and Steerable Features
   In [39], the right ventricle is extracted from cine Cardiac MR images using machine learning techniques, to ultimately build a statistical shape model that can predict RV remodelling at end diastole in patients with Tetralogy of Fallot (a congenital heart disease). A geometric model is used to segment the RV endocardium by first determining its orientation, position and scale in cine images automatically using Marginal Space Learning. A combination of Probabilistic Boosting Tree (PBT) and Haar like features along with steerable features is used for classification. The boundaries are then detected locally through the PBT and the statistical shape model. Manual correction is done where required. The ideal template that represents the population can be obtained from these surface meshes [40][41].

2.3. Cardiac Descriptors

Cardiac descriptors can be broadly classified into global or regional descriptors. Some examples of global descriptors are end systolic volume, end diastolic volume, ejection fraction and stroke volume while myocardial wall thickness is an example of local or regional parameter. The following section provides a list of descriptors that are found in this literature search along with normal values of some descriptors as mentioned in [42] and [43].

2.3.1. Traditional Cardiac Descriptors

Global Descriptors

1. LV End Diastolic Volume (LVEDV) and LV End Systolic Volume (LVESV): [44]-[22][23]-[31]:
   LVEDV is the volume of blood in the LV cavity when it is fully relaxed and when LVESV is volume of blood in the LV cavity when it is fully contracted. LVEDV and LVESV are sometimes indexed to

body surface area or height to allow comparisons between patients.

2. Left Ventricular Stroke Volume [45][26][11][22][23][25][12][29][19][31]:
It is defined as difference between the LVEDV and LVESV and represents the amount of blood ejected from the LV during a contraction.

$$StrokeVolume(LVSV) = LVEDV - LVESV$$

When indexed to the body surface area, the normal Stroke Volume Index is $45 \pm 8ml/m^2$

3. Left Ventricular Ejection Fraction [45]-[23][46]-[31]:
This cardiac parameter describes the volume of blood that is pumped out of the LV cavity. It is represented as a percentage and is given by:

$$EjectionFraction(LVEF) = \frac{LVEDV - LVESV}{LVEDV}$$

Normal Value: $67\% \pm 5\%$

4. Left Ventricular Mass [44][45][14][15][26][27][16][11][17][23][47][48][28][49][29][19][50][30]:
LV Mass is the mass of the myocardial tissue and is given by the product of the myocardial tissue density $(1.05g/cm^3)$ and the difference between the volume within the epicardium and LV cavity. Normal Value: $2.4 \pm 0.2g/kg$

5. Left Ventricular Cardiac Output [15][11] :
LV Cardiac Output is the product of the heart rate and LVSV and it describes the "systemic flow per minute". LV Cardiac Output is sometimes indexed to body surface area or height to allow comparisons between patients.

6. LV Index [44][15][16][49][29][19]:
The ratio of the LV mass to LV volume at end diastole is called LV Index and it is used for describing LV remodelling.

7. LV Sphericity Index:
LV length is defined as the ratio of the LVEDV and the volume of a sphere whose diameter is described as the longest axis of the left ventricle [26]. In [19], LV Sphericity index is defined as the ratio of distance between the apex and the mitral valve to the width of the LV at the level of the papillary muscles and is used as a measure to describe the geometrical remodelling of the LV.

8. LV Length[16]:
The distance between the apex and mitral valvular plane in a cine horizontal long axis image. Longitudinal contractility can be derived as the ratio of the difference between LV length at diastole and systole and the LV length at diastole.

9. LV Septal Lateral Delay [51]:
It is defined as the product of the frame delay and the temporal resolution and is used to describe mechanical dyssnchrony of the LV using cine Cardiac MR sequences. The temporal resolution is given by the inverse of the product of the R-R interval and frame-rate, while the frame delay is the number of frames between the beginning of septal thickening and lateral thickening during systole.

Local Descriptors

1. LV Wall Thickness:
The distance between the LV endocardial and epicardial contours gives an estimate of the LV Wall Thickness [20][26][48][49]. The center-line method describes the LV wall thickness through chords that are perpendicular to the centre-line and this method has also been extended to 3D by estimating the medial surface [42]. LV wall thickness can be used to further describe the LV cavity remodelling w.r.t LV myocardial remodelling by obtaining the ratio of the LV wall thickness and LV volume [26]. LV Relative Wall Thickness is defined as the ratio of the two times the infero-lateral wall thickness and the diameter of the left ventricle at end-daistole [44][47]. An asymmetry ratio that describes the asymmetric thickness of the myocardium can be derived as the ratio of maximum and minimum thickness in one slice [44].

2. Apical Conicity Ratio [52]:
   Apical Conicity Ratio is defined as the ratio of the volume of the apex at end-diastole to the volume of the cone with the height as the long axis of the apex and base described by the short axis area of the apical region. It is used as an index to describe LV apical geometry and the presence of LV aneurysms.

3. Systolic Dyssynchrony Index [20]:
   The Systolic Dyssynchrony Index is defined "as the standard deviation (SD) of the regional times to peak volume change, maximum muscle thickness or peak strain." The volume SDI is found to be a predictor for response of cardiac re-synchronization therapy.

4. Ventricular septum thickness [47]
   The authors do not mention the method used to estimate the inter-ventricular septum thickness.

5. Motion and Strain Analysis [42]:
   Motion analysis is performed by analysing point correspondences between landmarks that represent anatomical locations. Strain analysis is performed to describe myocardial deformation. This is done by considering the neighbouring point to estimate a deformation gradient tensor, which is then used to estimate shear and axial strains.

2.3.2. Non-Traditional Cardiac Descriptors

These descriptors help to describe the geometry of the left ventricle locally, but are not generally used in routine assessment as they are computationally intensive.

1. Geometric Descriptors

   (a) Curvature:
   The principal curvatures, k_1 and k_2, describe the maximum and minimum bending of a surface. The Gaussian curvature ($(k_1 + k_2)/2$) and mean curvature ($k_1.k_2$) are used for local geometrical analysis. [42].

   (b) Shape Index and Shape Spectrum:
   Shape index and curvedness are two parameters that are scale invariant (unlike the above parameters). Curvedness has been used to compare left ventricular geometry locally between healthy controls and patients with myocardial infarction in [24]. Shape index varies from -1 (for cup like umblic shapes) and +1 (for peak like umblic shapes). Shape Spectrum is derived from shape index and is defined as a fractional area of LV with a certain shape index at time *t*. SSPs can then be formed by connecting points that have the same shape index. Tracking these SSPs either locally or globally can provide insight into the geometry and motion of the left ventricle and also allow comparison with other pathologies [42].

   (c) Local Stretching:
   Local stretching of the LV epicardium is computed for corresponding patches of the LV epicardium before and after motion as the change in Gaussian curvature and a polynomial stretching model [42].

2. Model Specific Descriptors
   Global motion analysis based on deviation from an affine model: A polyhedral mesh of each time-frame is represented through moments and centre of mass. It is assumed that the motion induced differences between polyhedral meshes of different time-frames can be represented through affine transformations. To quantify the inter-frame variations, a corresponding deformation based on affine model is used to extract global motion parameters. This has then been used to distinguish between healthy controls and severely diseased LV. However, this method only provides a global analysis and not a localised analysis regarding the dysfunction of the LV [42].
   [42] describes methods to perform motion analysis through superquadric or other related models, and through planispheric transformation. Other descriptors like Geometric Cardiogram (GCG) and Deformation Spectrum can be obtained through model specific analysis of left ventricular geometry and function [42].

2.4. Methods Used to Estimate Cardiac Descriptors

Methods found in this review to estimate cardiac descriptors can be classified into computational template based approaches or geometrical template based approaches and this section describes these two approaches.

2.4.1. Computational Template Based Estimation

In [53], computational cardiac atlases which can be used to develop models to represent populations with a certain pathology, or to determine subject-specific functional models or to perform multi-modal image analysis for diagnosis are described. In their study, Cardiac MR image datasets consist of a large number of images, thus, limiting the analysis to global volume findings or qualitative regional assessment. Model based analysis uses mathematical models to quantify volume, regional wall motion and asynchronous LV contraction across populations with different pathologies and also offers the option to combine different imaging protocols. Model-based methods can be used to derive statistical descriptors of different cardiac parameters that allow comparison of patient specific models to healthy controls. Since computational atlases align all patient specific models to the same cardiac coordinate system, the point correspondence between shapes can be used to perform principal component analysis to represent any shape with a parameter that is weighted sum of the modes of deformation that describe the maximum variation and the mean model. Independent Component Analysis has been used to derive clinically relevant modes of deformation by determining the probability density function for each parameter (on a training set of healthy controls) and representing this probability density function of ICA elements in the spatial domain. Partial Least Square Regression is used to derive modes that are correlated with cardiac parameters is used for generating biomarkers to assess the aortic arch or the right ventricle [35][39].

2.4.2. Geometric Model Based Volume Estimation

In this literature search, it has been observed that almost all studies incorporate volume measurements while analyzing the LV function. Some of the studies used geometrical models to estimate LV volumes. An advantage of using geometrical models is the reduction in measurement and acquisition time. Geometrical models are used to analyse echocardiographic data and also for Cardiac MR data. [54] compares the performance of different geometrical models in estimating volumes from Cardiac MR data. LVEDV, LVESV, LVSV and LVEF are calculated using the methods/geometric models shown in Figure 2.2. The volume measurements obtained from the 3-D reconstruction or disc area summation method are used as the gold standard for comparing with the results from the geometrical models shown in Figure 2.2. The Modified Simpson's Method and Biplane ellipsoid are the most accurate and reproducible models, with a little underestimation from the results of Biplane ellipsoid model. The Hemisphere Cylinder model overestimated the volumes, thus, underestimating the LVEF, probably due to the difference in location of mitral valve and/or papillary muscles. The Single Plane Ellipsoid method showed better correlation with healthy controls compared to its correlation with patients. The Modified Teichholz formula underestimated volumes in most cases, especially in more spherical ventricles. The accuracy obtained from using geometrical models to estimate volumes is subject to the estimating the cross-sectional areas, especially near the middle of the ventricular cavity. Moreover, the geometrical models may not be very accurate in calculating volumes of ventricles with pathologies like ischemic cardiomyopathy as they do not account for LV remodelling.

2.5. Discussion

2.5.1. Pre-processing and segmentation techniques

The use of Cardiac MR for functional and geometrical analysis of the heart is increasing owing to its ability to accurately describe a wide range of cardiac descriptors. However, the accuracy of the analysis is affected due to the presence of artefacts induced from breathing motion and patient movement. This literature search presents techniques that are only based on image-based or geometry-based approaches. Further research to combine these techniques may help to compensate the disadvantages of the individual approaches [9]. The accuracy of the analysis also depends on the segmentation technique that is employed to generate the cardiac model from which the descriptors are estimated. This section discusses some of the factors that need to be considered while choosing between seg-

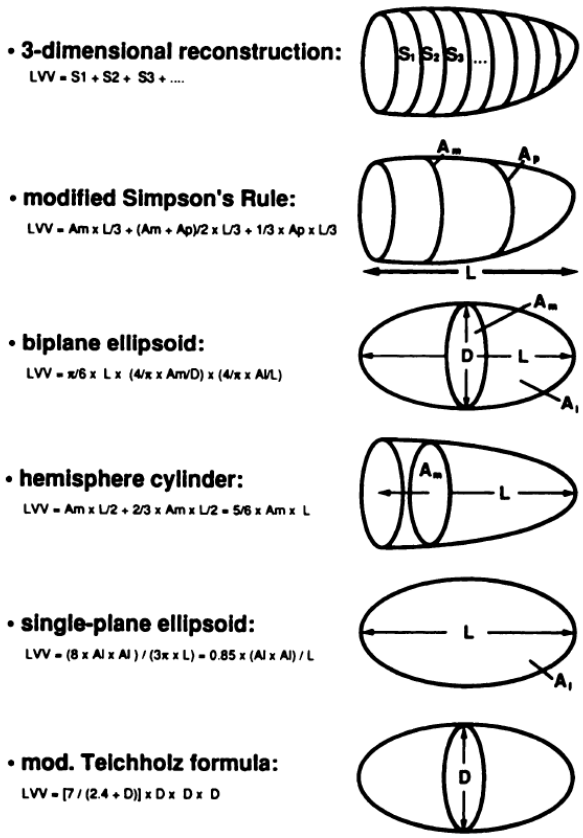

Figure 2.2: Geometrical models for volume measurements from cine Cardiac MR images.
Al: Largest LV cross-sectional area observed on a horizontal Long Axis image *Am:* LV cross-sectional area 1cm below the mitral valve *Ap:* LV cross-sectional area at the base of the papillary muscles *D:* LV cavity's diameter 1cm below the mitral valve *L:* Longest LV length observed in Long Axis (horizontal) plane *LVV:* LV Volume [54]

.

mentation techniques. The size of the data-set available for training or analysis plays an important role in selecting between manual, semi-automatic or automatic segmentation methods. When small data-sets are available, manual contour drawing may produce more accurate results. Though manual contour delineation is the most common technique used to segment the left ventricle, it can be very time-consuming (it takes about 2 hours for a trained professional to delineate an entire Cardiac MR data-set of 11 slices with 25 time-frames) and also be subject to inter/intra observer variability [36]. To circumvent these disadvantages, techniques based on active shape models, level sets, active appearance models, deformable models and atlas based approaches have been used to automate the process. However, semi automatic and automatic segmentation require large data-sets for training to produce models that incorporate higher subject variability to be applicable to larger populations. This is also observed in [34], where the volume is estimated incorrectly from the model for one patient whose volume is beyond the limit considered while building the shape model. Another criterion that needs to be considered while selecting a segmentation technique would be the level of accuracy required for a certain application. However, the parameters used to describe the segmentation accuracy and the imaging modalities from which the segmentation is obtained vary between studies. Thus, more standardized measures to describe accuracy are required to compare different methods [43].

2.5.2. Methods used to estimate cardiac descriptors

In this literature search, it is observed that several studies used manual contour delineation for segmenting and quantifying the left ventricular function. There is variation in the delineation methods used between studies - mainly with respect to including/excluding papillary muscles, myocardial tissue and LV outflow tract. The study presented in [55] describes the variabilities that are induced in volume

measurements owing to differences in methods used for contour delineation, basal slice identification and selection of end systolic and end-diastolic frame. Three scenarios - one with including the papillary muscles and trabeculae only for volume and not mass measurements, the second including the papillary muscles and trabeculae for both volume and mass measurements and third using a semi-automatic contour segmentation tool that included papillary muscles and trabeculae for mass but not volume measurements are compared with each other and also with the results from using geometrical models. The first scenario produced underestimated volume measurements compared to the other, especially for ESV measurement, probably owing to the compacted region available for delineation, though the simplified contour delineation is less time-consuming. This study observed that there is a poor agreement between the volume measurements obtained from geometrical models and the conventional analysis as the repeatability coefficients are 13% or higher when calculating the LVEF. These results contradict those obtained by [56]. According to [55], this disparity is because of the difference in parameters used to assess the performance of geometric models in both studies with [56] using "mean relative difference" which does not represent the confidence interval of the difference between techniques for an individual, but rather of the sample of individuals and [55] using the "absolute mean difference" obtained larger limits of agreement. This study presents the disadvantages in using geometrical models and advices to not use these geometrical models for Cardiac MR images owing to the real-world variabilites.
[57] provides standards and recommendations for qualitative and quantitative analysis of Cardiac MR images by the Task Force for the Post Processing of the Society for Cardiovascular MR (SCMR). According to this recommendations list, the papillary muscles, myocardial tissue and the LV outflow tract must be included as the blood pool while delineating contours for functional analysis. The most basal slice during systole can be selected by identifying the left atrium as either the cavity whose volume is increasing during systole or by the presence of myocardium in the blood pool and then considering the most basal slice with atleast 50% ventricular myocardium. However, the review presented in [43] states that there is no consensus to either include/exclude the papillary muscles from the blood pool. Appropriate normal values must be used for comparing between healthy controls and patient groups [55].
Use of deformable models, ASM or AAM and atlas-based approaches may help to circumvent these disadvantages by providing more robust and reproducible functional analysis. Computational cardiac atlases can produce a more encompassing functional and geometrical analysis of the cardiac chambers owing to their ability to be applied to different imaging modalities. The computational atlases can also be used to develop patient specific models by propagating the mean model to the image and using image evidence to stabilize the model. One of the major challenges for constructing computational atlases is the requirement for manual contour delineation for large data-sets, which can be very time-consuming. Recent developments towards building statistical models from imaging data should be extended to patient repositories to allow comparing healthy controls with disease specific subjects [53].

2.6. Conclusion

This literature review presents pre-processing techniques that can be used to correct breathing motion artefacts and segmentation techniques that are available to derive patient specific models for cardiac analysis. Cardiac descriptors are classified on the basis of their applicability in routine clinical assessment and methods used to estimate them are mentioned. Future work towards automating atlas computation and their applicability to larger databases with different patient subgroups may allow automatic identification of cardiac morphological patterns and the underlying pathophysiology [53].

3

Methods

This chapter provides an overview of the techniques used to simulate surgical ventricular reconstruction using the RMAS. The planning tool consists of several subsequent steps. First, the contours of the LV endocardium, epicardium and Right Ventricle are delineated on Cardiac MR cine images. Since the cine images of the heart are taken at different times, the 3D model may be affected by slice misalignment due to breathing motion and patient movement. The transformation required to correct for breathing artefacts and patient motion is estimated and applied to the original images. The scarred myocardium is identified on the contrast enhanced Cardiac MR image and is registered to the image stack of cine Cardiac MR images at end-diastole. Parts of the contour are classified based on their location with respect to the scar location. The healthy myocardium is simulated to represent the residual LV after the surgery. The effect of the surgery is subsequently quantified using functional and geometrical analysis. The success of the surgery is estimated through the following end-points:

- At least 30% reduction of end systolic and end diastolic volume
- Less than 40% obstruction of the RVOT by the plicated scarred myocardium

3.1. Image acquisition and contour delineation

Cardiac MR data-sets consisting of cine images and contrast enhanced images are acquired along different imaging planes using a Siemens 1.5T scanner. Cardiac imaging planes used in this study include the vertical long axis view (two-chamber view), LV outflow tract view (three-chamber view), horizontal long axis view (four chamber view) and the Short Axis (SA) planes. These planes extend from the LV apex to the centre of the mitral valve (long axis of the heart) on axial-plane images. The SA plane is perpendicular to the long axis of the heart at the mid-ventricular level. The number of SA slices obtained depends on the size of the LV. The four chamber plane is selected as the horizontal plane perpendicular to the short axis plane and the two-chamber plane is vertical plane perpendicular to the short axis plane [58]. The cine images acquired in all planes generally have 25 phases (time-frames) across the cardiac cycle. Figure 3.1 shows Cardiac MR images obtained along the different long-axis views. Example of a SA cine image along with the corresponding scar tissue is available in 1.1. These images are used to analyse LV function and also to identify and quantify the scarred myocardium. Different imaging planes are used to obtain a more accurate model of the LV thus, improving the quantitative analysis.
The endocarial, epicardial and right ventricular borders are manually delineated on the SA images along with the endocardium in the two- ,three- and four chamber views at end-diastolic and end-systolic phases using MASS (Medis, Leiden, The Netherlands) software by an experienced radiologist. As seen in Figure 3.2(a), the papillary muscles and the myocardial tissue are included in the endocardial border. Figure 3.2(b) shows a complete set of SA contours at end-diastolic and end-systolic phase.

3.2. Correction of breathing artefacts

A Cardiac MR image dataset generally suffers from slice misalignment due to breathing motion as the images are acquired over multiple breathing cycles and hence, at different diaphragm locations. More-

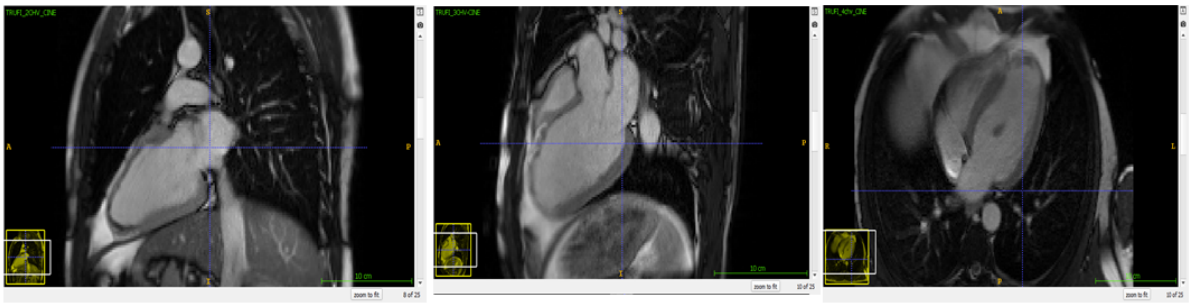

(a) (b) (c)

Figure 3.1: **(a)** Two- , **(b)** three - and **(c)** four - chamber views at diastole

.

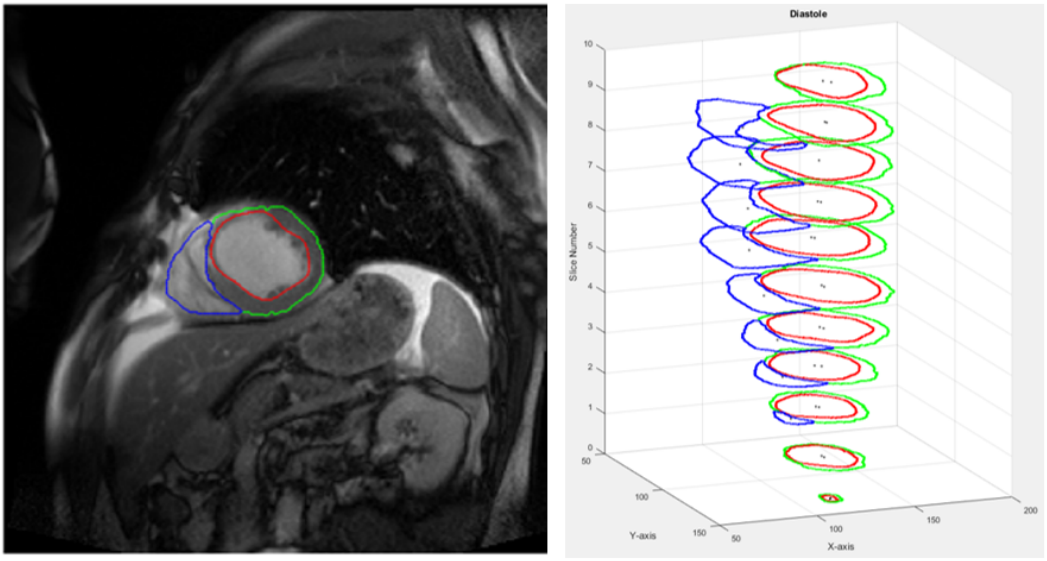

(a) (b)

Figure 3.2: Endocardial (red) , epicardial (green) and right ventricular (blue) contours drawn at **(a)** a SA slice **(b) The complete stack of SA contours showing endocardial (red) , epicardial (green) and right ventricular (blue) contours**

.

over, patient movement during the image acquisition further decreases the accuracy of the developed model [9]. The following section describes the method used to correct for in-plane misalignment introduced due to breathing motion and patient movement. The steps include registration of the contours into the patient coordinate system, down-sampling the long axis contours at the location of the closest SA planes, applying Iterative Closest Point Algorithm to obtain the required transformation of each SA contour to correct for in-plane breathing artefacts and applying the same on the original SA image.

Registration into the patient coordinate system

The endocardial, epicardial and right ventricular SA contours along with the contours of the endocardium in the two- ,three- and four chamber views at end-diastolic and end-systolic phases are registered into a three dimensional space described as the patient coordinate system using three image properties that are obtained from the DICOM tags - image position (DICOM tag - (0020,0032)), image orientation (Dicom tag - (0020,0037)) and pixel spacing (DICOM tag - (0028,0030)). The following

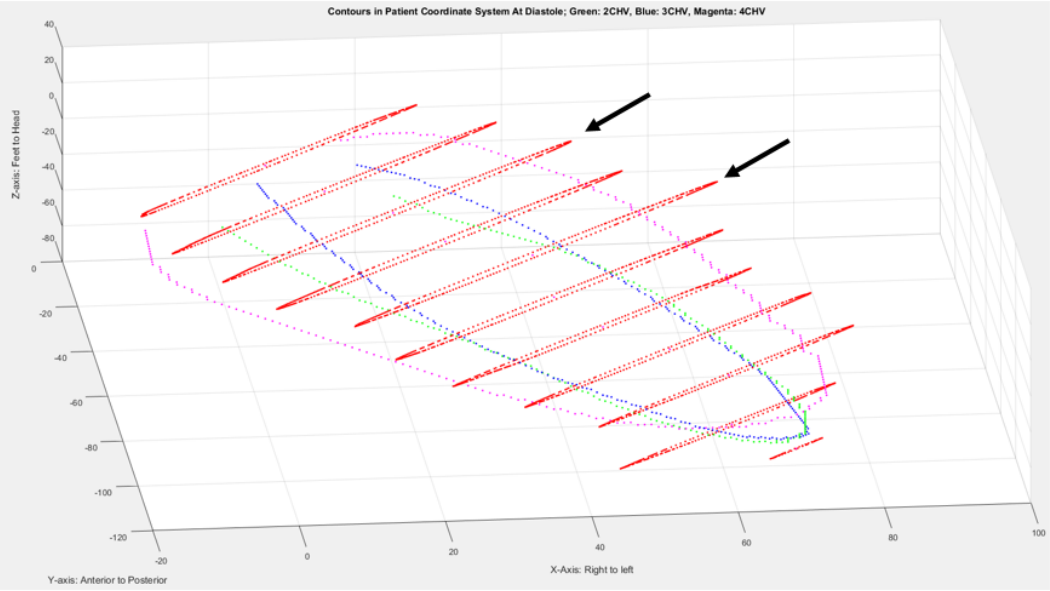

Figure 3.3: End-diastolic SA contours(red) along with two-chamber (green), three-chamber (blue) and four-chamber (magenta) contours projected into the Patient Coordinate System with black arrows pointing to slices that suffer from severe misalignment

.

transformation is used [59]

$$\begin{bmatrix} P_x \\ P_y \\ P_z \\ 1 \end{bmatrix} = \begin{bmatrix} X_x\Delta_i & Y_x\Delta_j & \frac{T_1^1 - T_1^N}{1-N} & T_1^1 \\ X_y\Delta_i & Y_y\Delta_j & \frac{T_2^1 - T_2^N}{1-N} & T_2^1 \\ X_z\Delta_i & Y_z\Delta_j & \frac{T_3^1 - T_3^N}{1-N} & T_3^1 \\ 0 & 0 & 0 & 1 \end{bmatrix} \begin{bmatrix} i \\ j \\ s \\ 1 \end{bmatrix} \tag{3.1}$$

where,
P_{xyz} = coordinates of the voxel in the Patient Coordinate System
X_{xyz} = row direction cosine component obtained from Image Orientation
Y_{xyz} = column direction cosine component obtained from Image Orientation
i = column index in the image plane
j = row index in the image plane
s = slice number of the image plane
N = number of slices
T^1 and T^N = image position of the most apical and most basal slice available in the slice set
Figure 3.3 shows the contours after they are projected into the patient coordinate system.

Down-sample long axis contours at the closest Short Axis planes

To account only for in-plane misalignment, the extent of the LV is determined on each SA plane by the the position of the long axis contours points that are closest to that SA plane. This section describes the steps incorporated to down-sample the contours of the two-, three- and four - chamber at the location of the closest SA planes. First, the SA plane corresponding to each contour is estimated. Four points of the two-, three- and the four- chamber contours that are closest to each SA plane are identified by computing the distance of each long axis contour point to every plane along the direction of the plane's normal. These four points are then projected onto the SA plane using the following equations (Figure 3.4):

$$t = \frac{(\mathbf{n} \cdot Point_1) - (\mathbf{n} \cdot Point_{LA})}{norm(\mathbf{n})} \tag{3.2}$$

$$x_0 = x + ta; y_0 = y + tb; z_0 = z + tc; \tag{3.3}$$

where, $[x_0, y_0, z_0]$ = LA point projected onto the SA plane
n = normal vector of the corresponding SA plane

$Point_1$ = point on the SA plane (mean of the contour points)
$Point_{LA}$ = one of the four LA points closest to the corresponding SA plane

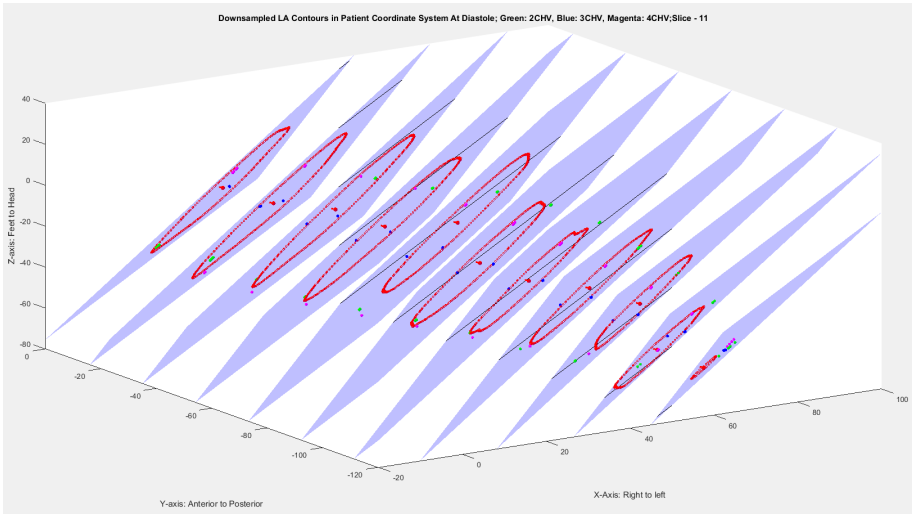

Figure 3.4: End-diastolic SA contours(red) along with two-chamber (green), three-chamber (blue) and four-chamber (magenta) contour points that have been down-sampled at the level of each SA plane projected into the Patient Coordinate System

.

Estimation and application of the transformation matrix

The SA contour points are registered to the down-sampled long axis points on each short axis plane using the Iterative Closest Point Algorithm. The Iterative Closest Point Algorithm performs a rigid registration (translation and rotation) to estimate the transformation matrix that minimizes the point-to-point distance between the SA contour points and the down-sampled LA points on the SA plane. Figure 3.5 shows the effect of applying the Iterative Closest Point Algorithm on the LV Endocardial contours. The transformation matrices obtained from the Iterative Closest Point algorithm are then

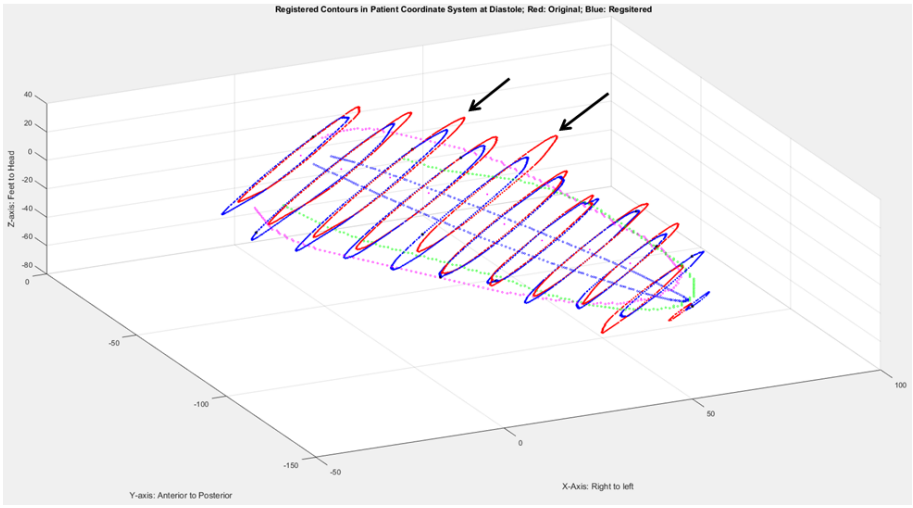

Figure 3.5: End-diastolic SA contours (red) along with the result of applying the Iterative Closest Point algorithm (blue) and the two-chamber (green), three-chamber (blue) and four-chamber (magenta) registered into the Patient Coordinate System with black arrows pointing to contours that were misaligned and have been corrected

.

applied to each SA image using `MeVisLab` network and the corrected images are combined to form a stack.

3.3. Estimation of Scar

The scarred region is visualised on contrast enhanced Cardiac MR images as a region with increased intensity and this is delineated using `ITK-SNAP` software [60]. To facilitate evaluation of scarred tissue on the SA contours, the contrast enhanced Cardiac MR image stack is registered to the stack of end-diastolic SA images obtained from the previous step. The registration is performed in two steps - a rigid followed by an affine registration using `elastix` software. Multi-resolution registration is performed at 5 resolutions, a gradient descent optimiser with an adaptive gain is used as the optimiser and Normalised Mutual Information is used as a similarity metric. The segmentation of the scarred myocardium is transformed to the space of the fixed image (stack of SA images at end-diastole) using `transformix` [61][62].

There is a need to establish point-to-point correspondence between SA contours across different slices, so as to allow identification of scar location and extent, and to build a 3D model of the LV. To establish point to point correspondence, the angle each contour point of a SA contour makes with the x-axis is first determined. The difference between the angles of consecutive contour points is determined. The contour point at the index of the minimum difference is selected as the first contour point and the other contour points are re-ordered accordingly. The contour points are then sampled at 64 angle points. This process is repeated for all SA contour slices.

To identify the location of the scar on a short axis contour, the transformed scar is visualized along with the contour on the SA image of the corresponding slice (Figure 3.6).

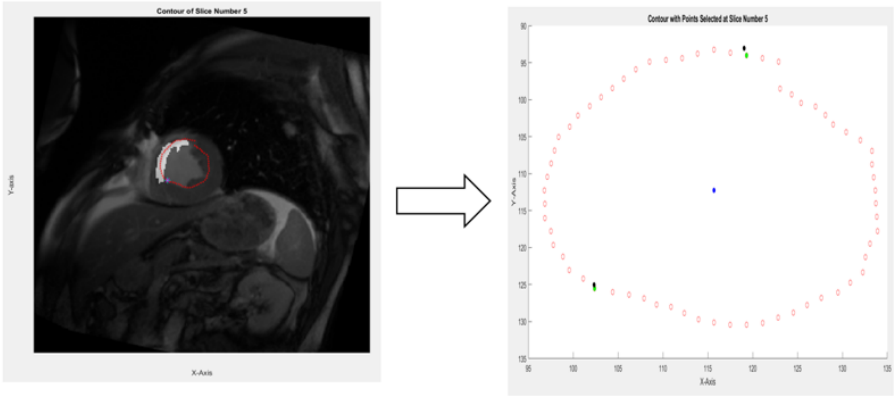

(a) (b)

Figure 3.6: **(a)** SA endocardial contour visualized on the image of the corresponding SA along with the scar segmentation of that slice.**(b)** Points describing the extremity of the scar tissue are highlighted. (Black - points selected by the user and green - closet contour points that are selected)

.

Two points that describe the extent of the scar along the decreasing y-direction are manually selected. Each contour point is then given a label based on its location when compared to the manually selected scar extremities. Figure 3.7 shows the SA contour set highlighting the scarred region in both Image Coordinate System and the Patient Coordinate System. The length of the scar tissue is determined at each SA slice as the sum of distances between consecutive sampled contour points with the scar label. The length of the healthy myocardium is also determined by computing as the difference between the scar length and the distance between all consecutive contour points.

3.4. Simulation of surgical ventricular reconstruction

To simulate the procedure of reconstruction through RMAS, three assumptions are made. Firstly, it is assumed that the anchors are placed at every SA slice, thus, modifying the geometry of each SA contour that has been identified to have a scarred segment. Secondly, it is assumed that the scarred segment of the SA contour is plicated such that it forms a circle, also, leaving behind a circle of healthy myocardial segment. The centre of the scarred segment is calculated, and it is assumed that the scarred segment is plicated such that it plicates at this point 3.8.

The circumference of the SA contour is first calculated to be say, L units and it is then represented

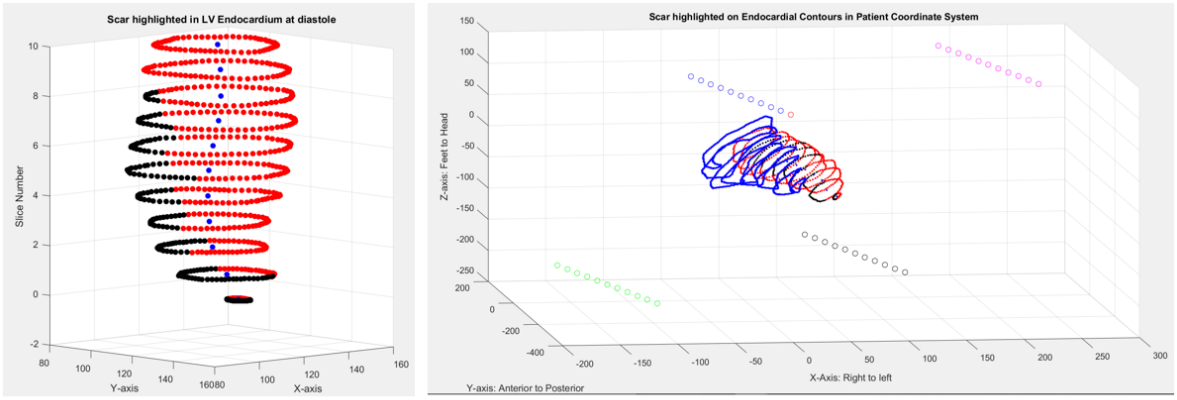

(a) (b)

Figure 3.7: Scarred tissue located in the inter-ventricular region highlighted on SA contours in **(a)** Image Coordinate System and **(b)** Patient Coordinate System. (Right ventricular contours - blue, healthy LV endocardial contours - red and scarred tissue - black

.

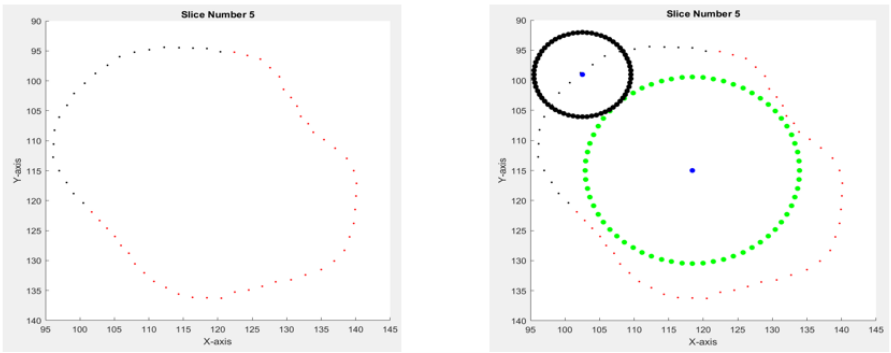

(a) (b)

Figure 3.8: **(a)**Original SA contour with the scar highlighted **(b)** Simulation of the surgical ventricular reconstruction on a SA contours

.

as two segments, namely, the scar (L_{scar} units) and the healthy segment ($L_{healthy}$ units). The circle of the residual SA contour and the scarred segment are obtained by considering the length of the corresponding segments to be the circumference of that circle. The circle of the residual SA contour at both end-diastolic and end-systolic frame are placed at the center of mass of the SA contour of that slice at the end-diastolic phase. The centre of the scar circle is determined by identifying the angle at which the centre of the scarred segment is sampled on the original SA contour and then translating the center along that angle by the radius of the scar circle. Figure 3.9 shows a simulation on the set of SA contours in both Image Coordinate System and the Patient Coordinate System. To visualize and quantify the effect of the simulation on the geometry of the residual LV, surface models of the SA contours before and after simulation are generated. This is achieved by triangulating the contour points such that the normal of each patch points outwards. The vertices are contained in a [N X 3] matrix, where N is the total number of contour points in the entire stack and faces describe the triangular connectivity of these vertices.

3.5. Analysis

This section describes the methods used to quantify the residual LV by comparing its function with the baseline characteristics and analysing its geometry.

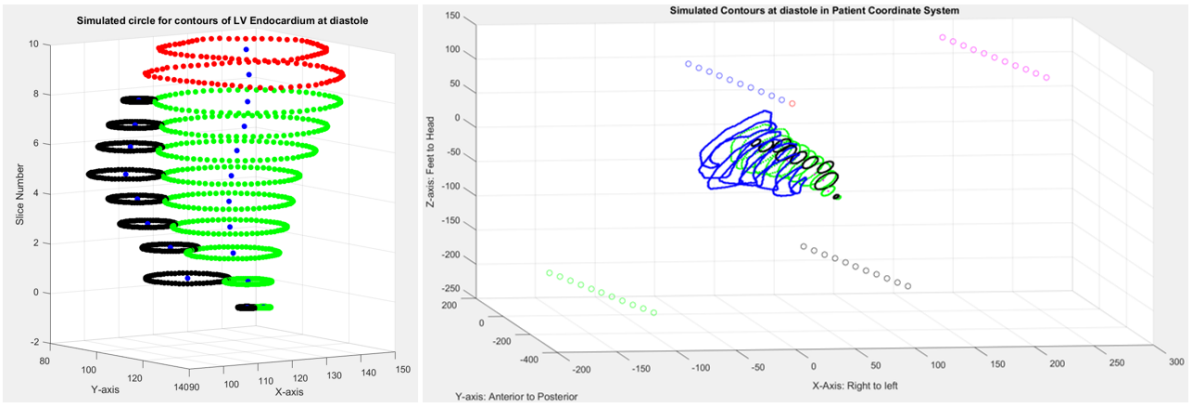

(a) (b)

Figure 3.9: Simulation of the RMAS on SA contours in (a) Image Coordinate System and (b) Patient Coordinate System. (Right ventricular contours - blue, healthy LV endocardial contours - green and scarred tissue - black

3.5.1. Functional Analysis

Four parameters - LVEDV, LVESV, Stroke Volume and Ejection Fraction are used for functional analysis of the LV. To determine the volume at a time-frame, the area enclosed by each SA contour is calculated and is multiplied by the sum of slice thickness and slice gap. The sum of volumes obtained from all slices is considered to be the volume of the LV at that time-frame. The scar volume at the end-systolic and the end-diastolic phase is also obtained with the same procedure. Stroke Volume and Ejection Fraction are estimated as mentioned in the previous chapter. The values of the pre-surgical and post-surgical LV are compared with the baseline characteristics obtained from the MASS (Medis, Leiden, The Netherlands) software.

3.5.2. Geometrical Analysis

Geometrical analysis of the effect of the LV reconstruction involves quantification of the amount of occlusion of the RVOT by the plicated scar and comparison of the geometry of the residual LV with other LV geometrical models. The amount of RVOT obstruction is estimated by first defining the extent (diameter) of the RVOT at the most basal slice the right ventricular contours are defined at. It is assumed that the RVOT forms a circular annulus and this circle is estimated from the user defined extent. The overlap between the circular annulus of the RVOT and the scar circle at that slice is calculated 3.10.

According to [55], the Modified Simpson's Model and the Biplane Ellipsoid Model are the most accurate

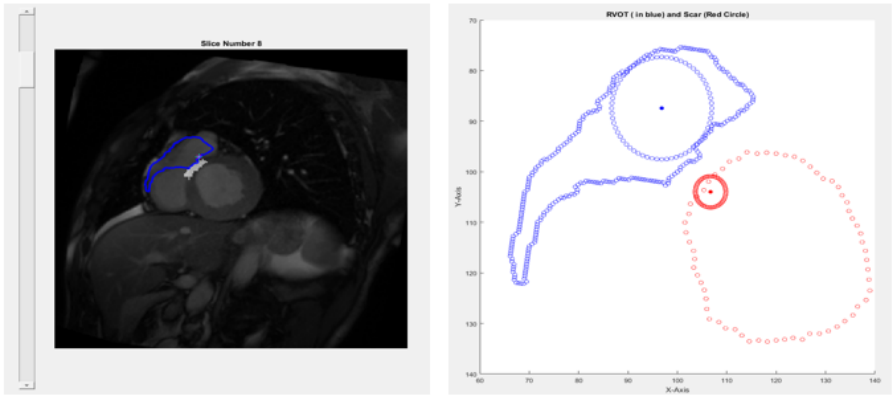

(a) (b)

Figure 3.10: **(a)** Most basal right ventricular contour visualised on the corresponding Cardiac MR image to select the extent of the RVOT **(b)** Estimation of the RVOT annulus along with scar circle at the slice

and reproducible geometrical models for volume measurements, compared to the other models. Hence, in this study, these models are constructed and the curvedness is used to compare these models with the residual LV. As shown in Figure 2.2, the Modified Simpson's Model describes the LV as a combination of a cylinder from the base of the LV to the mitral valve, a truncated cone from the mitral valve to the base of the papillary muscles and a cone until the apex. On the other hand, the Biplane Ellipsoid Model describes the LV as an ellipsoid using the length of the LV and the cross-sectional area of the LV 1cm below the leaflets of the mitral valve in the short-axis view.
In [24], time series of a surface shape descriptor called curvedness is used as an index to quantify geometrical remodelling in the LV after a myocardial infarction and also to distinguish patients from a control group. In this study, the triangulated meshes of the residual LV and those of the geometrical models are compared using curvedness. The principal curvatures k_1 and k_2 are obtained by fitting a quadratic surface to a local region of the LV and are used to define curvedness as shown in equation 3.4:

$$C = \sqrt{\frac{k_1^2 + k_2^2}{2}} \tag{3.4}$$

The curvedness value obtained at each vertex is subsequently compared with the value at the corresponding vertex of both the geometrical models.

4

Results

A total of 4 male patients between the age-group of 49-69 years with ejection fraction less than 40% are studied, with one of the patients having both pre- and post surgery scans. Cardiac MR data is used as the imaging modality for pre-surgery scans of three patients except one (who had a CT scan due to the presence of a pacemaker). A graphic user interface is built on `Matlab` that guides the user sequentially through the steps mentioned in the previous chapter. Figure 4.1 shows a few screen-shots of the same.

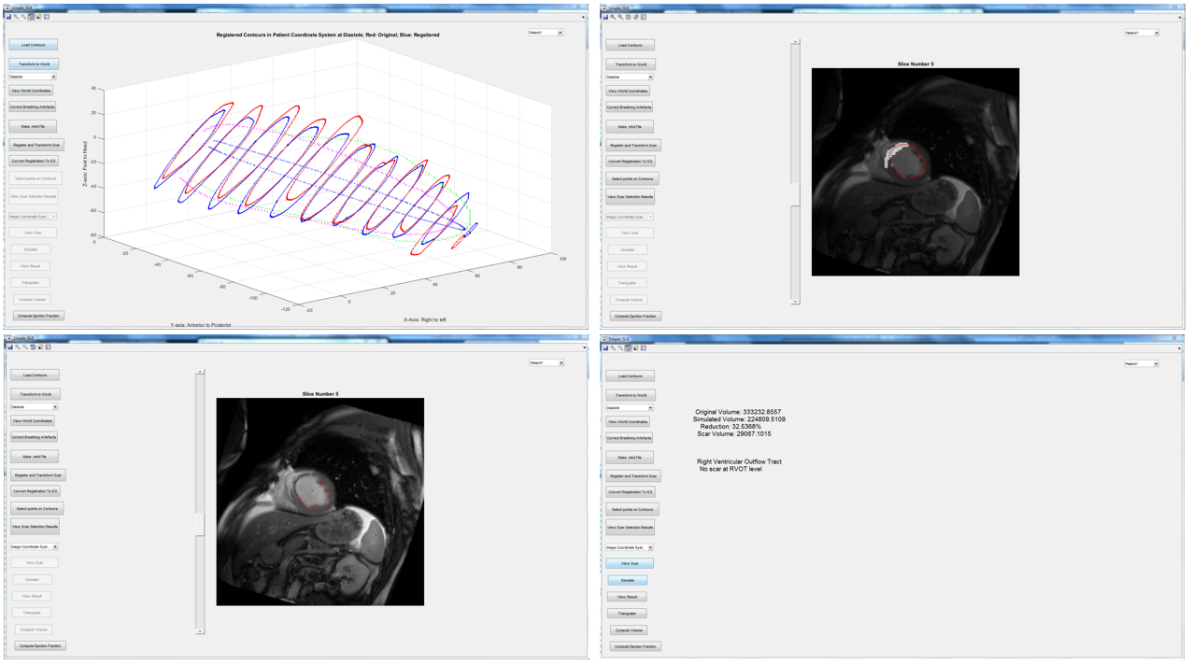

Figure 4.1: Screenshots of the Graphic User Interface

This chapter first describes the results of the method used to correct for breathing motion and patient movement induced artefacts, followed by the results of simulation and of the quantification.

4.1. Correction of breathing artefacts

This method is applied on all the patients who have Cardiac MR data. The SA contours before and after correction are triangulated and Figure 4.2 shows the effect of the method on the contours and also on the SA image stack.

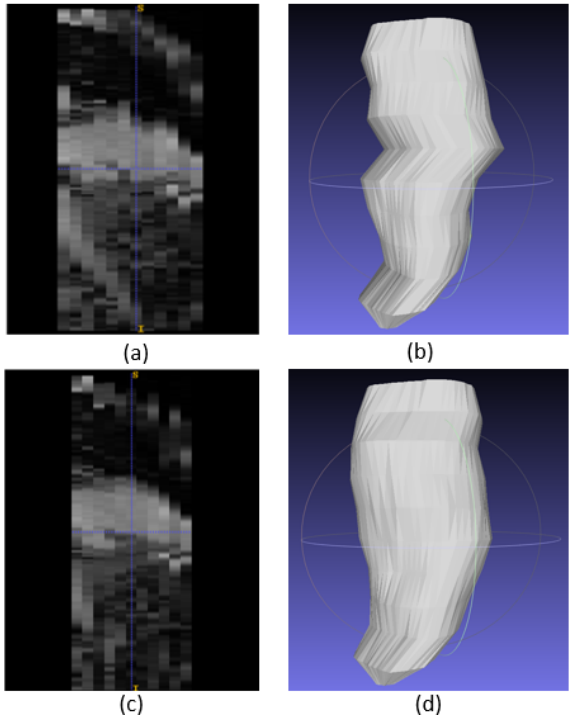

Figure 4.2: Result of method to correct for breathing and patient movement artefacts. **(a)** Stack of SA images before correction and **(b)** surface model generated from contours before correction. **(c)** Stack of SA images after correction and **(d)** surface model generated from contours after correction.

4.2. Simulation

Figure 4.3 shows the triangulated surface of the contours before and after simulation at end-diastole for all the patients.

4.3. Analysis

4.3.1. Functional Analysis

The LV volumes at systole and diastole obtained from the method described in the previous chapter are compared with the values obtained from the MASS software in Table 4.1. The stroke volumes and ejection fractions are also compared with the values obtained from MASS software in Table 4.2. The contour method mostly agrees with the MASS estimate with a minimum difference of 0.18% and maximum of 14.5%. The stroke volume produced a minimum difference of -1.1% and a maximum difference of 18.5% The difference in the ejection fraction is in the range of 1.6% to 11.9%.

Table 4.3 shows the difference in the volume of the scar estimated at the end systolic and end diastolic phase. Table 4.4 and Table 4.5 show the reduction in functional characteristics of the simulated residual LV compared to the baseline characteristics obtained from the MASS estimate and the contour method. The reduction in the volumes obtained at end-systolic and end-diastolic phase meet the requirements of the surgery.

Table 4.1: Comparison between LV volumes obtained from the MASS software and the contour method at end-systolic and end-diastolic phase

Pat. No.	End Systolic Volume (ml)			End Diastolic Volume (ml)		
	MASS Estimate	Contour Method Estimate	Difference	MASS Estimate	Contour Method Estimate	Difference
1	187	211.3	13%	291	333.2	14.5%
2	110	111.6	1.45%	178	172.2	-3.27%
3	272	272.7	0.26	290	290.5	0.18%
4	483	456.4	-5.52%	585	563.6	-3.65

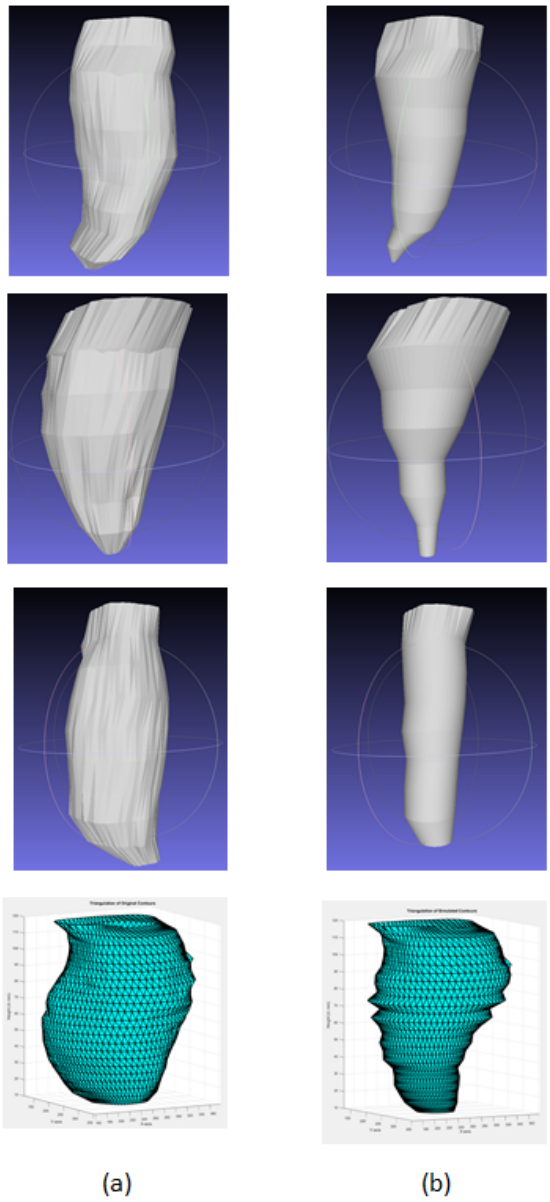

Figure 4.3: Triangulated surface obtained from **(a)** original contours and **(b)** simulated contours at end-diastolic phase for all patients.
The triangulation of LV models of Patient 4 when exported to mesh lab produced a scaling defect, and hence, the result of visualization in `matlab` is displayed

.

Table 4.2: Comparison between LV stroke volume and ejection fraction obtained from the MASS software and the contour method at end-systolic and end-diastolic phase

Pat. No.	Stroke Volume (ml)			Ejection Fraction (%)		
	MASS Estimate	Contour Method Estimate	Difference	MASS Estimate	Contour Method Estimate	Difference
1	103	122	18.4%	36	36.6	1.69%
2	67	60	-9.58%	38	35.2	7.40%
3	18	17.8	-1.11%	6	6.1	2.17%
4	102	107.3	5.19%	17	19	11.9%

The results of the functional analysis performed for the post-surgical scans of one patient are compared with those obtained from MASS software in Table 4.6.

Table 4.3: Difference in scar volume estimated at end-systolic and end-diastolic phase

Pat No	Scar Volume (ml)		
	Systole (ml)	Diastole (ml)	Difference (%)
1	31.4	29.4	-6.97
2	21.4	26.6	19.7
3	73.4	69.9	-4.90
4	48.1	52.2	7.95

Table 4.4: Comparison of reduction of LVESV and LVEDV of the simulated residual LV with the baseline characteristics estimated by MASS software and Contour Method

Pat No	End Systolic Volume (ml)			End Diastolic Volume (ml)		
	Simulated Volume (ml)	Reduction (%)		Simulated Volume (ml)	Reduction (%)	
		MASS Estimate	Contour Method Estimate		MASS Estimate	Contour Method Estimate
1	119.1	36.3	43.6	224.6	22.8	32.6
2	64.6	41.8	42.0	107.9	39.4	37.3
3	124.1	54.4	54.5	141.2	51.3	51.4
4	303.2	37.1	33.6	398	32.0	29.4

Table 4.5: Comparison between LV stroke volume and ejection fraction obtained from the simulation with baseline characteristics estimated from MASS software and contour method

Pat No	Stroke Volume (ml)			Ejection Fraction (%)		
	Simulated Volume (ml)	Difference (%)		Simulated Ejection Fraction (%)	Difference (%)	
		MASS Estimate	Contour Method Estimate		MASS Estimate	Contour Method Estimate
1	105.5	2.43	- 15.6	47.0	30.5	28.3
2	43.3	-35.4	- 28.5	40.1	5.61	12.3
3	17.1	-5.09	- 4.03	12.1	100.2	95.8
4	94.9	-6.97	-11.6	23.8	40.2	25.3

Table 4.6: Comparison of the post-operative functional analysis with the result of simulation

	MASS Estimate	Image Estimate	Difference (%)	
			Image Estimate	Simulation
End Systolic Volume (ml)	150	156.1	4.09	17.3
End Diastolic Volume (ml)	218	198.9	- 8.76	35.2
Stroke Volume (ml)	68	42.8	37.1	75
Ejection Fraction (%)	31	21.5	30.65	61

4.3.2. Geometrical Analysis

Figure 4.4 shows the surface plots of the simulated residual LV models of all the patients and the residual LV model derived from the post-surgical scan of one patient at the end-diastolic phase highlighting the curvedness values. Figure 4.5 shows the curvedness values of the Modified Simpson's Model and the Biplane Ellipsoid Model obtained for each patient. Table 4.7 shows the mean and standard deviation of the simulated LV models of all patients and the residual post-surgical LV of one patient and the mean and standard deviation of the difference obtained while comparing these models with their corresponding geometrical models.

Table 4.7: Mean and standard deviation of curvedness values (mm^{-1}) of the simulated residual LV of all patients and the residual post-surgical LV model of one patient along with the mean and standard deviation of the difference obtained when comparing these models with their corresponding geometrical models

Patient Number		Residual LV Model (Mean, Standard deviation)	Difference	
			Modified Simpson Model (Mean, Standard deviation)	Biplane Ellipsoid Model (Mean, Standard deviation)
1		0.0414 ±0.0458	0.0157 ±0.0448	- 0.0028 ±0.0488
2		0.0582 ±0.0816	0.0253 ±0.0871	0.0175 ±0.0826
3	Simulated LV	0.0513 ±0.0304	0.0005 ±0.0307	- 0.0205 ±0.0307
	Post-surgical LV	0.0315 ±0.0353	0.0225 ±0.0331	0.0229 ±0.0329
4		0.0222 ±0.018	-0.0001 ±0.0204	0.0084 ±0.0203

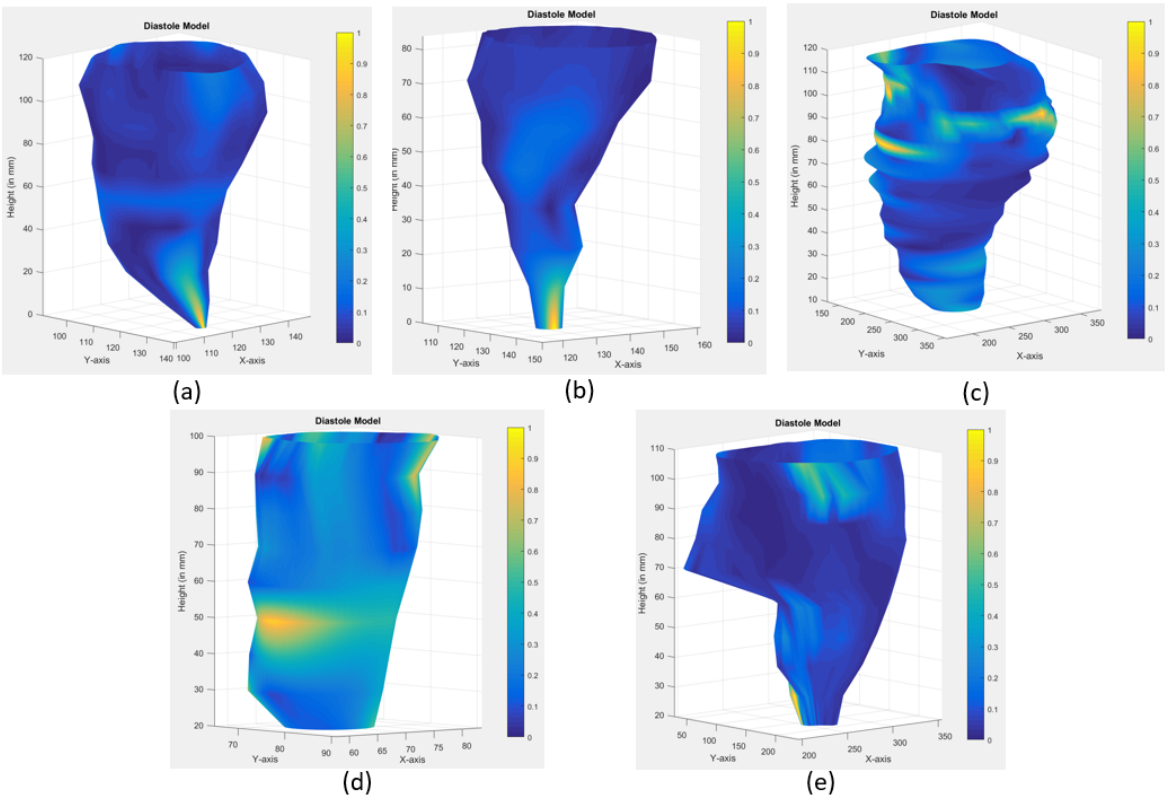

Figure 4.4: Surface plots of simulated residual LV Models highlighting curvedness values normalised between 0 and 1 for **(a)** Patient 1 **(b)** Patient 2 **(c)** Patient 4 **(d)** Patient 3 **(e)** post surgical model of Patient 3

.

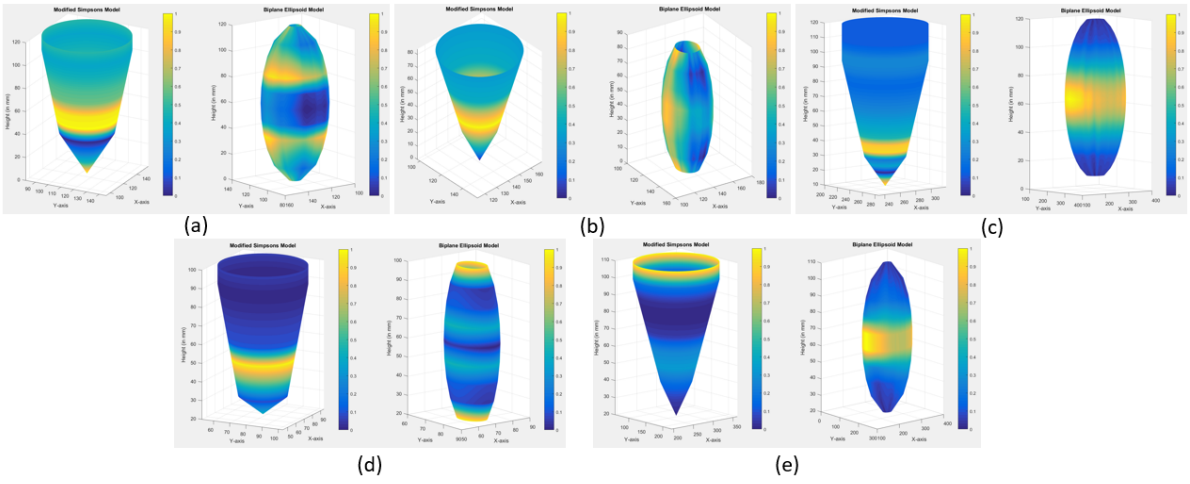

Figure 4.5: Surface plots of geometrical LV Models highlighting curvedness values normalised between 0 and 1 for **(a)** Patient 1 **(b)** Patient 2 **(c)** Patient 4 **(d)** Patient 3 **(e)** post surgical model of Patient 3 obtained after removing the segments that contain leakage of contrast

.

5

Discussion

In this study, a planning tool that allows *in silico* modelling of SVR by RMAS is developed whilst this procedure has been introduced in clinical practice. All developments and considerations whilst introducing this procedure can be included into this tool. Functional improvement is characterised by at least 30% decrease in LVEDV and LVESV and also a maximum of 40% obstruction of RVOT. The method has been used on all four patients, and when comparing the functional outcomes of the simulated residual LV, it is observed that the required end-points of the procedure for functional improvement are met for all patients when comparing these characteristics with the baseline characteristics obtained from either the contour method or from the MASS software.

5.1. Pre-processing techniques

Pre-processing techniques to correct for breathing motion artefacts were validated through visual examination of the LV shape. Figure 4.2 shows the improvement in the geometrical structure of the LV of one patient. After realignment of SA contours, the distortion in the LV structure has decreased. This can also be visualised by comparing the image stacks as the corrected image stack produces a smoother transition between slices.
However, there are two main drawbacks with this approach. Firstly, it has been observed in some patients that the long axis contours are not completely defined at all regions, thus, leading to inaccurate registrations (Figure 5.1). In this study, the slices at which the LA contours are not completely defined are not modified to correct for breathing artefacts - they are copied without modification into the new image stack. The study presented in [9], uses an iterative approach to register the SA contours to the set of long axis contours and to register long axis contours to a set of SA contours. This iterative process, when restricted to only in-plane movement of contours, may help to improve the accuracy of the model obtained. Secondly, in this study, the improvement in the quality of the model after correcting breathing artefacts is not quantitatively analyzed. Comparing the intersection of the model with the long axis images and the contours of the long axis images before and after correction can by used as a parameter as shown in [9].

5.2. Simulation

Previous studies that analysed the effect of LV reconstruction through RMAS did not use a simulation tool to estimate the effect of the surgery [4][5]. To the best of our knowledge, this is the first tool developed to aid in the planning of LV reconstruction through RMAS. The simulation technique used in this study implements an ideal method to plicate the scar by folding the scarred myocardium at its center at the level of every SA slice. However, this technique has a few drawbacks. Firstly, the assumption that only the scar tissue at each SA slice level is completely plicated, may not be practical at all slice locations due to the presence of other cardiac structures, which are not accounted for in this study. Figure 5.2 shows the segmentation of the LV obtained from the post-surgery scan at the end-diastolic phase which shows the leakage of contrast into the plicated region. This indicates that the scar could not be completely plicated in this patient due to the presence of the conduction system

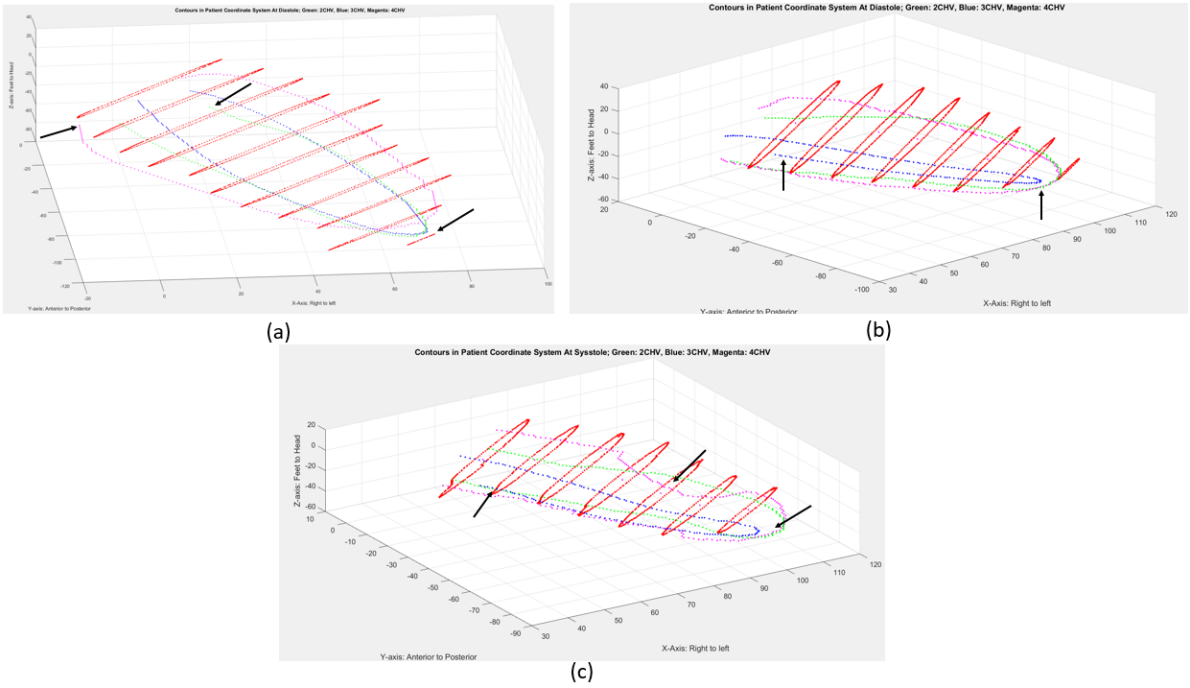

Figure 5.1: Contours in the Patient Coordinate System with black arrows pointing to instances where the delineated long axis contours are not defined at SA slice locations

.

of the heart. In addition, it is not practical to place anchors at each SA slice level (8mm-12mm). This may be required when the scar length and/or location varies between slice levels. In such situations, a part of the healthy myocardium can also be plicated. Moreover, the shape of the residual LV at each slice level and the change in the location of the center of the residual LV must be analysed by comparing with a larger data-sets. This will help to understand the effect of the reconstruction on the other cardiac structures, thus, providing a more comprehensive understanding of the surgery. Lastly, the effect of stress induced due to the placement of anchors on the myocardium and movement of the anchors is not accounted for in this planning tool as was considered in the initial ovine studies of [5].

5.2.1. Functional Analysis

Functional analysis of the LV includes evaluating four parameters - LVEDV, LVESV, estroke volume and jection fraction. The volume estimation of patient 1 presents a larger difference (Table 4.1) compared to the other patients. This difference in estimation of volumes is also propagated to a difference in the estimation of stroke volume, but is not present in the estimation of ejection fraction. This patient could also be an outlier - which can be verified by using a larger database of patients.

Table 4.3 also shows some discrepancy in the scar volume that is observed between end systolic and end diastolic phase, even when the same scar segmentation is used for delineation. This can be attributed to the fact that the scar is manually delineated on each slice. Moreover, in Patient 2, the difference in the scar volume is also because the most apical contour is not defined at the end-systolic phase to account for movement of LV during contraction.

Previous study performed on one patient observed a reduction of greater than 50% in the LVESV and LVEDV immediately after the surgery. A slight improvement of ejection fraction immediately after the surgery and 39% improvement six months after the surgery was observed. In another study conducted on 11 patients, a percent reduction of 36.2 ±18.3 and 39.6 ±14.8 in the LVESV and 28.6 ±18.8 and 21.2 ±14.9 in the LVEDV was observed 6 and 12 months respectively. In this study, while comparing the reduction in simulated residual LV volume at end diastolic and end-systolic phase, a higher reduction at the end-systolic phase is observed. This can be expected as the result of the registration between the contrast enhanced MR and the cine Cardiac MR image stack at the end-diastolic phase is used without modification to delineate scar at the end-systolic phase, to account for the ischemic nature of the

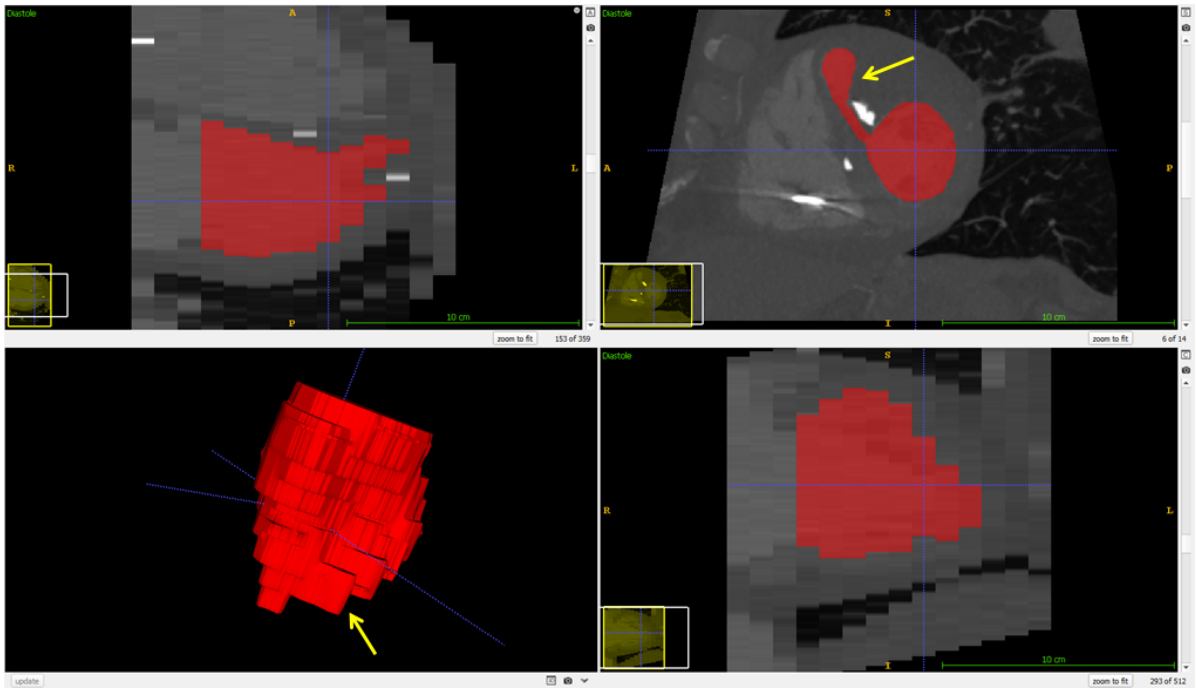

Figure 5.2: Segmentation of the LV obtained from a post-operative scan showing leakage of contrast into the plicated region (pointed by yellow arrows)

scar. Almost all patients for whom the baseline volume characteristics were overestimated, the volume reduction is also overestimated. All simulations produced the required reductions when compared to the baseline characteristics estimated by the MASS software or those estimated by the contour method. A reduction in stroke volume and an associated increase in the ejection fraction is also observed (4.5). The post-operative scan of one patient has been used to derive functional characteristics which have been compared with those obtained from the simulation. Table 4.6 shows that the volume is largely under-estimated in the simulation when compared to the post-operative scenario. This can be attributed to the fact that the simulation assumes complete plication of the scar. However as shown in Figure 5.2, there is leakage of contrast into the plicated region, indicating incomplete plication. There is a large difference in the ejection fraction estimated by simulation and the post-operative scan. The simulation calculates the ejection fraction based on difference in the area enclosed by the healthy segment of the contours at end-diastole and end-systole. The length of the healthy segment is obtained after delineation of the scar segment. As the ejection fraction of this patient is extremely low, there will be little difference in the length of the contour at end-diastole and end-systole. By plicating the same amount of the scar segment from both time-frames, the ejection fraction is under-estimated. However, in the post-surgical scenario, the contraction of the healthy myocardium produces the ejection fraction, unlike in the simulation where the difference in the contour segment is used to produce the ejection fraction. The accuracy of these results can be validated by comparing the post-operative data with those of the simulations produced by an experienced radiologist on larger databases.

5.2.2. Geometrical Analysis

No occlusion of the RVOT by the plicated scar has been observed in any patient in this study. However, the results need to be validated by accounting for the change in the location of the right ventricle due to the plication, so to provide a more realistic estimation of the occlusion. This can be done through intensity based methods on the Cardiac MR image dataset.

The geometry of the residual LV model is analysed by comparing the curvedness values at each vertex of the LV model with that obtained at the corresponding vertex of the patient-specific geometrical models. Curvature information has been used for quantitative regional analysis of the LV in [63] [64], and has shown to provide accurate results. The choice to use curvedness as the shape based descriptor by [24] over the more common curvature based descriptors like Gaussian curvature and mean curvature

stemmed from the observations that these descriptors can sometimes be misleading. The Gaussian curvature fails to describe extent of curvature in toroidal surfaces as it depends on the intrinsic geometry of the surface. The mean curvature at a saddle point is zero, even though the surface is curved. On the other hand, curvedness value is the magnitude of curvature at a point on the surface, and thus, can be used to measure the "degree of curvature at a point"[65]. Moreover, curvedness can be easily extended to estimate 3-D wall stress as shown in [65].
However, there are three major drawbacks with this analysis, due to which it is not possible to accurately interpret the results. Firstly, by calculating the mean and standard deviation of the entire model, the local changes in geometry are not accounted for. Due to this, it is difficult to select the geometrical model, that best describes the simulation of the surgery. Using the 16-segment LV heart model as in [24] to produce localised time series of curvedness values, can produce more accurate results. Secondly, the selection of slices that indicate 1cm below the mitral valve leaflet, base of the papillary muscle and the length of the LV need to be annotated by an experienced radiologist, to allow more uniformity and accuracy in the geometrical models that are produced. Lastly, larger databases of pre-surgical and corresponding post-surgical scans, can help to identify the ideal geometrical model more accurately.

6

Conclusion

Surgical ventricular reconstruction is a treatment modality that is used for patients with severe ICM. RMAS is a reconstruction technique that aims to restore the LV geometry and function by plicating the scarred region with anchors. Due to the minimally invasive nature of the procedure, surgical planning mainly depends on pre-procedural imaging rather than on peri-procedural imaging. This study develops an *in-silico* modelling tool that simulates the effect of the reconstruction to allow functional and geometrical analysis of the residual LV.

The planning tool developed in this study corrects for slice mis-alignment caused from breathing motion and patient movement. Location of the anchors is selected at all short axis slice levels that contain scarred tissue. Functional analysis includes determination of the LV volume at the end-diastolic and end-systolic phase, stroke volume and ejection fraction. The baseline LV characteristics are compared with the results of the simulated LV. Geometrical analysis includes quantifying the overlap of the occlusion of the RVOT by the plicated scar and comparison of the curvedness values obtained at each contour point of the simulated residual LV model and the geometrical models. The required end-points for the procedure are atleast 30% reduction in the LV volume at the end-diastolic and end-systolic phase when compared with baseline characteristics and at most 40% occlusion of the RVOT. By changing the location of the anchors, the user can simulate different residual LV models and analyse their function and geometry.

The accuracy of the results obtained in this study needs to be validated by comparing the residual LV models that are generated from the anchor locations that are selected by an experienced radiologist and the post-surgical LV models for large datasets. Moreover, the improvement in the LV models after the pre-processing step also needs to be quantitatively analysed.

Acquiring contrast enhanced images at all time frames instead of only at the end-diastolic phase can help to reduce the registration errors that are introduced while defining the scar location and extent. The accuracy of the simulation can be improved by considering other cardiac structures like the conduction system of the heart while selecting the anchor positions. In addition, simulation on large datasets can help to understand and quantify the effect of the reconstruction on the other cardiac structures, thus, simulating more realistic residual LV models. Larger datasets can be used to build a statistical shape model of the post-surgical residual LV that can be used to obtain a more encompassing understanding of the effect of reconstruction on both function and geometry of the residual LV.

7

Appendix

The *in-silico* planning tool for the Revivent Myocardial Anchoring System is implemented on `Matlab 2016b` and a Graphic User Interface (GUI) is developed to guide the user sequentially through the steps described in the "Methods" section. Before implementing the GUI on `Matlab`, the DICOM cine Cardiac MR images at the end-systolic and end-diastolic phases are stored in folders called `Systole` and `Diastole` respectively. The DICOM files are converted to `.mhd` format using the `Praxis` tool. The `.mhd` files are combined to form one `.mhd` file ensuring that the apical slice is the first slice and is stored in the corresponding folder. The folder of each patient also contains the short axis and long axis contours.

Inputs to the Graphic User Interface:

The GUI requires the user to select the patient whose data needs to be evaluated. This selection can be performed on the drop-down list located on the top-right corner. The `Load Contours` button is activated and it allows the user to select the long axis contour files (two-chamber, three-chamber and the four-chamber views) and the SA contour files. The SA contours (LV Endocardium, LV Epicardium and RV) are then displayed at the end-systolic and end-diastolic phase in the Image Coordinate System. The `Transform to World` button is then activated and when selected allows the user to select the folders containing the two-chamber, three - chamber, four-chamber DICOM images and the folder with the SA DICOM images at the end-diastolic phase. The GUI requires the slice number corresponding to the most apical and most basal slice. By selecting the time frame (either systole or diastole), all the contours of that time-frame can be viewed by selecting the `View World Coordinates`. The GUI also provides a tool to rotate the figures. The button to correct for breathing artefacts is activated.

Pre-Processing to correct for breathing motion and patient movement:

On selecting the `Correct Breathing Artifacts` button, planes corresponding to the SA contours are estimated by normalizing all SA contours points by their corresponding mean values. Eigen analysis is performed on the covariance matrix obtained from the reduced points and the principal directions are extracted to obtain the normal to each plane. The normals of all SA planes are aligned to point in the cranial direction. The SA planes are then be obtained using the normal and the point on the plane (mean of each SA contour). The algorithm estimates the extent of LV on each SA plane as described in the "Methods" section. Iterative Closed Point Algorithm to estimate the transformation matrix that minimizes the point-to-point distance between the SA contour points and the down-sampled LA points on each SA plane is implemented using an inbuilt function called `pceregrigid`.
The `Make mhd file` button is activated and when selected, makes a folder in either the `Systole` or `Diastole` (depending on the chosen time-frame), called `BreathingCorrection`. The apical and basal slices that are present in the SA contour set are then given as input and the algorithm makes sub-folders corresponding to these slice numbers. The transformation matrices obtained from the Iterative Closest Point algorithm are applied to each SA image using `MeVisLab` network and the

corrected images are combined to form a stack. A schematic representation of this network is shown in Figure 7.1. Firstly, the `.mhd` files of the original slices are loaded into the `itkImageFileReader` network in `MevsiLab` and the transformation matrix is applied to the World Coordinate System of the image. Image slices with different orientation information may not be stored as a single volume and to circumvent this issue, the result obtained from applying the transformation matrix is registered into the the World Coordinate System of the original image. Each slice is then saved as a DICOM file. After applying the transformation to all SA images, checking the box on the screen allows the user to convert each SA DICOM file into a `.mhd` file and to combine all the individual slices into a file called `BreathTrial.mhd`. This file is then used as input to the `MeVisLab` network and saved as `BreathTrialCorrect.mhd` in the same folder after correcting for the sub-voxel shift.

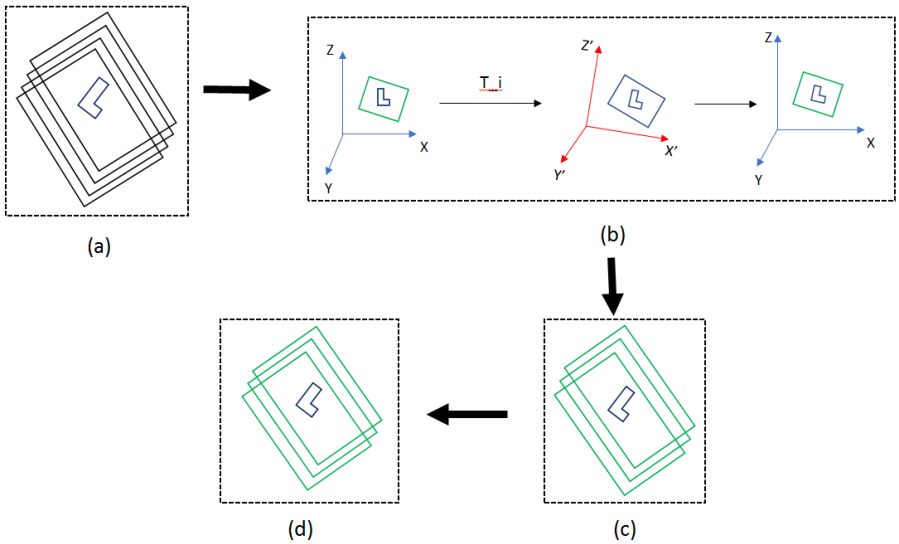

Figure 7.1: Schematic representation of the approached used to correct breathing motion artefacts on image data. The `.mhd` file obtained from the DICOM file **(a)** is transformed using the transformation matrix obtained from the Iterative Closest Point algorithm and then registered into the World Coordinate System of the original image **(b)** and is saved as a DICOM image. The stack of DICOM images are converted into a single `.mhd` file **(c)** and the stack of SA images is saved again after correcting for sub-voxel shift **(d)**

.

Scar estimation and delineation

By selecting the `Register and Transform Files` button, the algorithm performs the registration process described in Section 3.3. This step requires the user to define a binary region of interest and save it in the appropriate `BreathingCorrection` folder as `BreathingMask.mhd`. The results of the registration are stored in `RegisteredBreathing` folder in the `Diastole` folder as the contrast enhanced image is only registered to the end-diastolic phase. The user is then indicated to change the order of the "FinalBSplineInterpolationOrder" in the `TransformParameters.0` and in the `TransformParameters.1` to 0, after which the algorithm transforms the scar segmentation from the contrast enhanced image space to the fixed image space (image stack at the end-diastolic phase). On selecting the `Convert Registration to ICS`, the SA contours that have been corrected for breathing motion and patient movement are converted into the Image Coordinate System using the inverse of the transform matrix estimated for the SA DICOM images.

`Select Scar on Contours` displays the result of the transformation on the appropriate SA image and allows the user to place the anchor points in the decreasing y-direction. The second anchor point is selected by a double click. The SA contours are then classified into healthy or scarred regions based on their location with respect to the anchor points. The most basal right ventricular contour is also displayed on the corresponding slice, if the scar is present at that level. This allows the user to define the extent of the RVOT's annulus.

`View Scar Selection` plots the SA contours on the corresponding SA image highlighting the scarred region in black and the healthy region in red. The user can then select between Image Coordinate

System and Patient Coordinate System in the drop-down list and the scar can be visualized in the appropriate coordinate system.

Simulation

On selecting the `Simulate` button on the GUI, the algorithm computes the length of the scar and healthy segments. These lengths are used as circumference of the circle that represents the contour of the residual LV. The occlusion of the RVOT (if the scar is present at the RVOT level) is calculated as the overlap between the binary masks of the residual LV and the RVOT annulus. The amount of overlap is displayed on the GUI. `View Results` allows the user to visualize the results of the simulations in the coordinate system selected in the drop-down list. `Triangulate` button triangulates the contour points such that the normal of each patch points outwards. The vertices are contained in a [N X 3] matrix, where N is the total number of contour points in the entire stack and faces describe the triangular connectivity of these vertices. Two sets of triangles are formed - one estimating the surface between consecutive slices from lower slice to the higher slice and the other estimating the surface in the opposite direction. The `Triangulate` button produces triangulation of the original contours, the contours that have been corrected for breathing motion and patient movement and the simulated contours that represent the residual LV. These triangulations are stored in either `Systole` or `Diastole` folder (depending on the chosen time-frame) in `.stl` format [66]. The results of the triangulation can also be visualized on the GUI.

Functional Analysis

`Compute Volume` determines the volume at the selected time-frame. Each SA contour is first convert into a binary image. The area enclosed by the contour at each SA slice is computed as the product of the number of pixels contained within the contour (obtained from the `bwarea` function), the pixel spacing in the x- direction and the pixel spacing in the y-direction. The area is then multiplied by the sum of slice thickness and slice gap. The sum of volume obtained from all slices is considered to be the volume of the LV at that time-frame. The volume of the original LV, simulated residual LV, the reduction in LV volume and the scar volume are displayed on the GUI. After obtaining the volume at both the time-frames, the original and simulated stroke volume and ejection fraction are computed and displayed on the GUI on selecting the `Compute Ejection Fraction` button. The most basal contour of the second patient is excluded from the volume computation. It represents the level of the LV Outflow Tract and when included in the volume measurements, produced overestimations compared to the volume measuements obtained from the MASS software.

Geometrical Analysis - Curvedness

The slice numbers corresponding to 1cm below the level of the mitral valve and the base of the papillary muscle (selected here as 1 slice apical to the slice that displays papillary muscles) are provided as input. The Modified Simpson's model is constructed as a combination of a cylinder (from the most basal SA contour to the the level of the mitral valve), a truncated cone (from the level of the mitral valve to the base of the papillary muscles) and a cone (from the base of the papillary muscles to the apex of the LV). The truncated cone and the cone are placed at the centre of the contour at the level of the mitral valve. To construct the Biplane Ellipsoid model, an ellipse is fit to the contour at the level of the mitral valve. The semi-major and semi-minor axes obtained from the `regionprops` function along with half the length of the LV (determined from the number of slices, slice thickness and slice gap) are used to construct the model using `ellipsoid` function. The model is placed at the center of the SA contour at the mitral valve, but translated to the vertical center of the LV (obtained from the number of slices). The contours at each slice level are obtained from the `contour` function. The geometrical models (sampled at 64 angle points) and the simulated residual LV models are triangulated.
`patchcurvature` [67] is used to determine the principal curvatures at each vertex using third order neighbourhood. The principal curvatures are used to determine the curvedness value of each vertex. These values are normalized between 0 and 1 to produce the visualizations. The difference is computed on the original curvedness values and is normalized for visualization.

Bibliography

[1] Wikipedia, *Ischemic cardiomyopathy,* (2017).

[2] N. Briceno, A. Schuster, M. Lumley, and D. Perera, *Ischaemic cardiomyopathy: pathophysiology, assessment and the role of revascularisation,* Heart **102**, 397 (2016).

[3] A. C. To and M. Y. Desai, *Role of cardiac magnetic resonance imaging in assessing ischemic and nonischemic cardiomyopathies,* Expert review of cardiovascular therapy **10**, 223 (2012).

[4] J. Liu, Z. Liu, Q. Zhao, A. Chen, Z. Wang, and D. Zhu, *Role of surgical ventricular restoration in the treatment of ischemic cardiomyopathy,* The Annals of thoracic surgery **95**, 1315 (2013).

[5] S. Castelvecchio, L. Menicanti, and M. D. Donato, *Surgical ventricular restoration to reverse left ventricular remodeling,* Current cardiology reviews **6**, 15 (2010).

[6] R. Faria, B. Melica, G. Pires-Morais, A. Rodrigues, J. Ribeiro, M. Guerra, V. Gama, and L. Vouga, *New less invasive ventricular reconstruction technique in the treatment of ischemic heart failure,* Revista Portuguesa de Cardiologia (English Edition) **33**, 469 (2014).

[7] A. S. Wechsler, J. Sadowski, B. Kapelak, K. Bartus, G. Kalinauskas, K. Rucinskas, R. Samalavicius, and L. Annest, *Durability of epicardial ventricular restoration without ventriculotomy,* European Journal of Cardio-Thoracic Surgery **44**, e189 (2013).

[8] S. M. Adhyapak, P. G. Menon, and V. Rao Parachuri, *Restoration of optimal ellipsoid left ventricular geometry: lessons learnt from in silico surgical modelling,* Interactive cardiovascular and thoracic surgery **18**, 153 (2013).

[9] M. Wan, W. Huang, J.-M. Zhang, X. Zhao, J. C. Allen, R. San Tan, X. Wan, and L. Zhong, *Correcting motion in multiplanar cardiac magnetic resonance images,* Biomedical engineering online **15**, 93 (2016).

[10] M.-L. Tan, Y. Su, C.-W. Lim, S. K. Selvaraj, L. Zhong, and R.-S. Tan, *A geometrical approach for automatic shape restoration of the left ventricle,* PloS one **8**, e68615 (2013).

[11] J. Andersson, C. Mellberg, J. Otten, M. Ryberg, D. Rinnström, C. Larsson, B. Lindahl, J. Hauksson, B. Johansson, and T. Olsson, *Left ventricular remodelling changes without concomitant loss of myocardial fat after long-term dietary intervention,* International journal of cardiology **216**, 92 (2016).

[12] E. Di Cesare, S. Battisti, A. Di Sibio, P. Cipriani, R. Giacomelli, V. Liakouli, P. Ruscitti, and C. Masciocchi, *Early assessment of sub-clinical cardiac involvement in systemic sclerosis (ssc) using delayed enhancement cardiac magnetic resonance (ce-mri),* European journal of radiology **82**, e268 (2013).

[13] T. A. Fairbairn, C. D. Steadman, A. N. Mather, M. Motwani, D. J. Blackman, S. Plein, G. P. McCann, and J. P. Greenwood, *Assessment of valve haemodynamics, reverse ventricular remodelling and myocardial fibrosis following transcatheter aortic valve implantation compared to surgical aortic valve replacement: a cardiovascular magnetic resonance study,* Heart **99**, 1185 (2013).

[14] A. Barison, L. Gargani, D. De Marchi, G. D. Aquaro, S. Guiducci, E. Picano, M. M. Cerinic, and A. Pingitore, *Early myocardial and skeletal muscle interstitial remodelling in systemic sclerosis: insights from extracellular volume quantification using cardiovascular magnetic resonance,* European Heart Journal-Cardiovascular Imaging **16**, 74 (2014).

[15] E. B. Turkbey, N. W. Jorgensen, W. Johnson, A. G. Bertoni, J. F. Polak, A. D. Roux, R. P. Tracy, J. A. Lima, and D. A. Bluemke, *Physical activity and physiological cardiac remodelling in a community setting: the multi-ethnic study of atherosclerosis (mesa),* Heart **96**, 42 (2010).

[16] W. Utz, S. Engeli, S. Haufe, P. Kast, M. Hermsdorf, S. Wiesner, M. Pofahl, J. Traber, F. C. Luft, M. Boschmann, *et al.*, *Myocardial steatosis, cardiac remodelling and fitness in insulin-sensitive and insulin-resistant obese women,* Heart **97**, 1585 (2011).

[17] W. Chasseriaud, E. Gerbaud, M. Montaudon, S. Gilbert, H. Cochet, Y. Pucheu, A. Horovitz, J. Bonnet, H. Douard, and P. Coste, *Effect of ivabradine on left ventricular remodelling after reperfused myocardial infarction: a pilot study,* European Heart Journal **34**, P1329 (2013).

[18] M. Sohal, S. Amraoui, Z. Chen, E. Sammut, T. Jackson, M. Wright, M. O'Neill, J. Gill, G. Carr-White, C. A. Rinaldi, *et al.*, *Combined identification of septal flash and absence of myocardial scar by cardiac magnetic resonance imaging improves prediction of response to cardiac resynchronization therapy,* Journal of Interventional Cardiac Electrophysiology **40**, 179 (2014).

[19] C. Chrysochou, M. Schmitt, K. Siddals, J. Hudson, A. Fitchet, and P. A. Kalra, *Reverse cardiac remodelling and renal functional improvement following bilateral renal artery stenting for flash pulmonary oedema,* Nephrology Dialysis Transplantation **28**, 479 (2012).

[20] M. Sohal, S. G. Duckett, X. Zhuang, W. Shi, M. Ginks, A. Shetty, E. Sammut, S. Kozerke, S. Niederer, N. Smith, *et al.*, *A prospective evaluation of cardiovascular magnetic resonance measures of dyssynchrony in the prediction of response to cardiac resynchronization therapy,* Journal of Cardiovascular Magnetic Resonance **16**, 58 (2014).

[21] D. Carrick, C. Haig, S. Rauhalammi, N. Ahmed, I. Mordi, M. McEntegart, M. C. Petrie, H. Eteiba, S. Hood, S. Watkins, *et al.*, *Prognostic significance of infarct core pathology revealed by quantitative non-contrast in comparison with contrast cardiac magnetic resonance imaging in reperfused st-elevation myocardial infarction survivors,* European heart journal **37**, 1044 (2015).

[22] B. N. Putko, H. Yogasundaram, K. Chow, J. Pagano, A. Khan, D. I. Paterson, R. B. Thompson, and G. Y. Oudit, *Normal left-atrial structure and function despite concentric left-ventricular remodelling in a cohort of patients with anderson–fabry disease,* European Heart Journal-Cardiovascular Imaging **16**, 1129 (2015).

[23] A. Palazzuoli, M. Beltrami, L. Gennari, A. G. Dastidar, R. Nuti, E. McAlindon, G. D. Angelini, and C. Bucciarelli-Ducci, *The impact of infarct size on regional and global left ventricular systolic function: a cardiac magnetic resonance imaging study,* The international journal of cardiovascular imaging **31**, 1037 (2015).

[24] M. Wan, T. S. Kng, X. Yang, J.-M. Zhang, X. Zhao, W. S. Thai, C. L. C. Wan, L. Zhong, R. San Tan, and Y. Su, *Left ventricular regional shape dynamics analysis by three-dimensional cardiac magnetic resonance imaging associated with left ventricular function in first-time myocardial infarction patients,* in *Engineering in Medicine and Biology Society (EMBC), 2014 36th Annual International Conference of the IEEE* (IEEE, 2014) pp. 5113–5116.

[25] H. Latus, K. Gummel, K. Klingel, A. Moysich, M. Khalil, N. Mazhari, J. Bauer, R. Kandolf, D. Schranz, and C. Apitz, *Focal myocardial fibrosis assessed by late gadolinium enhancement cardiovascular magnetic resonance in children and adolescents with dilated cardiomyopathy,* Journal of Cardiovascular Magnetic Resonance **17**, 34 (2015).

[26] J. Ganame, G. Messalli, P. G. Masci, S. Dymarkowski, K. Abbasi, F. Van de Werf, S. Janssens, and J. Bogaert, *Time course of infarct healing and left ventricular remodelling in patients with reperfused st segment elevation myocardial infarction using comprehensive magnetic resonance imaging,* European radiology **21**, 693 (2011).

[27] E. Canali, P. Masci, J. Bogaert, C. Bucciarelli Ducci, M. Francone, E. McAlindon, I. Carbone, M. Lombardi, W. Desmet, S. Janssens, *et al.*, *Impact of gender differences on myocardial salvage and post-ischaemic left ventricular remodelling after primary coronary angioplasty: new insights from cardiovascular magnetic resonance,* European Heart Journal–Cardiovascular Imaging **13**, 948 (2012).

[28] H. Watabe, A. Sato, H. Nishina, T. Hoshi, A. Sugano, Y. Kakefuda, Y. Takaiwa, H. Aihara, Y. Fumikura, Y. Noguchi, *et al.*, *Enhancement patterns detected by multidetector computed tomography are associated with microvascular obstruction and left ventricular remodelling in patients with acute myocardial infarction,* European heart journal **37**, 684 (2015).

[29] O. J. Rider, A. Lewandowski, R. Nethononda, S. E. Petersen, J. M. Francis, A. Pitcher, C. J. Holloway, S. Dass, R. Banerjee, J. P. Byrne, *et al.*, *Gender-specific differences in left ventricular remodelling in obesity: insights from cardiovascular magnetic resonance imaging,* European heart journal **34**, 292 (2012).

[30] E. Wu, J. T. Ortiz, P. Tejedor, D. C. Lee, C. Bucciarelli-Ducci, P. Kansal, J. C. Carr, T. A. Holly, D. Lloyd-Jones, F. J. Klocke, *et al.*, *Infarct size by contrast enhanced cardiac magnetic resonance is a stronger predictor of outcomes than left ventricular ejection fraction or end-systolic volume index: prospective cohort study,* Heart **94**, 730 (2008).

[31] A. J. Swift, D. Capener, C. Hammerton, S. M. Thomas, C. Elliot, R. Condliffe, J. M. Wild, and D. G. Kiely, *Right ventricular sex differences in patients with idiopathic pulmonary arterial hypertension characterised by magnetic resonance imaging: pair-matched case controlled study,* PloS one **10**, e0127415 (2015).

[32] P. Lamata, M. Sinclair, E. Kerfoot, A. Lee, A. Crozier, B. Blazevic, S. Land, A. J. Lewandowski, D. Barber, S. Niederer, *et al.*, *An automatic service for the personalization of ventricular cardiac meshes,* Journal of The Royal Society Interface **11**, 20131023 (2014).

[33] E. Theofilogiannakos, G. Theofilogiannakos, P. Danias, T. Yioultsis, A. Anogeianaki, V. Stergiou-Michailidou, K. Kallaras, T. Xenos, and G. Anogianakis, *A semi-automated approach towards generating three-dimensional mesh of the heart using a hybrid mri/histology database,* Computer methods in biomechanics and biomedical engineering **14**, 349 (2011).

[34] E. G. Caiani, A. Colombo, M. Pepi, C. Piazzese, F. Maffessanti, R. M. Lang, and M. C. Carminati, *Three-dimensional left ventricular segmentation from magnetic resonance imaging for patient-specific modelling purposes,* Europace **16**, iv96 (2014).

[35] J. L. Bruse, K. McLeod, G. Biglino, H. N. Ntsinjana, C. Capelli, T.-Y. Hsia, M. Sermesant, X. Pennec, A. M. Taylor, and S. Schievano, *A statistical shape modelling framework to extract 3d shape biomarkers from medical imaging data: assessing arch morphology of repaired coarctation of the aorta,* BMC medical imaging **16**, 40 (2016).

[36] L. Zhong, J.-M. Zhang, X. Zhao, R. San Tan, and M. Wan, *Automatic localization of the left ventricle from cardiac cine magnetic resonance imaging: a new spectrum-based computer-aided tool,* PloS one **9**, e92382 (2014).

[37] A. K. Shetty, S. G. Duckett, M. R. Ginks, Y. Ma, M. Sohal, J. Bostock, S. Kapetanakis, J. P. Singh, K. Rhode, M. Wright, *et al.*, *Cardiac magnetic resonance-derived anatomy, scar, and dyssynchrony fused with fluoroscopy to guide lv lead placement in cardiac resynchronization therapy: a comparison with acute haemodynamic measures and echocardiographic reverse remodelling,* European Heart Journal–Cardiovascular Imaging **14**, 692 (2012).

[38] J. Peters, O. Ecabert, C. Meyer, H. Schramm, R. Kneser, A. Groth, and J. Weese, *Automatic whole heart segmentation in static magnetic resonance image volumes,* in *International Conference on Medical Image Computing and Computer-Assisted Intervention* (Springer, 2007) pp. 402–410.

[39] T. Mansi, I. Voigt, B. Leonardi, X. Pennec, S. Durrleman, M. Sermesant, H. Delingette, A. M. Taylor, Y. Boudjemline, G. Pongiglione, *et al.*, *A statistical model for quantification and prediction of cardiac remodelling: Application to tetralogy of fallot,* IEEE transactions on medical imaging **30**, 1605 (2011).

[40] Y. Zheng, A. Barbu, B. Georgescu, M. Scheuering, and D. Comaniciu, *Four-chamber heart modeling and automatic segmentation for 3-d cardiac ct volumes using marginal space learning and steerable features,* IEEE transactions on medical imaging **27**, 1668 (2008).

[41] Z. Tu, *Probabilistic boosting-tree: Learning discriminative models for classification, recognition, and clustering,* in *Computer Vision, 2005. ICCV 2005. Tenth IEEE International Conference on*, Vol. 2 (IEEE, 2005) pp. 1589–1596.

[42] A. F. Frangi, W. J. Niessen, and M. A. Viergever, *Three-dimensional modeling for functional analysis of cardiac images, a review,* IEEE transactions on medical imaging **20**, 2 (2001).

[43] P. Peng, K. Lekadir, A. Gooya, L. Shao, S. E. Petersen, and A. F. Frangi, *A review of heart chamber segmentation for structural and functional analysis using cardiac magnetic resonance imaging,* Magnetic Resonance Materials in Physics, Biology and Medicine **29**, 155 (2016).

[44] E. Pozo, A. Kanwar, R. Deochand, J. M. Castellano, T. Naib, P. Pazos-López, K. Osman, M. Cham, J. Narula, V. Fuster, *et al.*, *Cardiac magnetic resonance evaluation of left ventricular remodelling distribution in cardiac amyloidosis,* Heart **100**, 1688 (2014).

[45] P. J. Ngu, M. Butler, A. Pham, S. K. Roberts, and A. J. Taylor, *Cardiac remodelling identified by cardiovascular magnetic resonance in patients with hepatitis c infection and liver disease,* The international journal of cardiovascular imaging **32**, 629 (2016).

[46] C. Manhenke, T. Ueland, B. I. Jugdutt, K. Godang, P. Aukrust, K. Dickstein, and S. Ørn, *The relationship between markers of extracellular cardiac matrix turnover: infarct healing and left ventricular remodelling following primary pci in patients with first-time stemi,* European heart journal **35**, 395 (2014).

[47] N. Partanen, M. Husso, O. Vuolteenaho, P. Sipola, H. Ruskoaho, K. Peuhkurinen, and J. Magga, *N-terminal pro-atrial natriuretic peptide reflects cardiac remodelling in stage 1 hypertension,* Journal of human hypertension **25**, 746 (2011).

[48] G. Ashrafpoor, E. Bollache, A. Redheuil, A. De Cesare, A. Giron, C. Defrance, A. Azarine, L. Perdrix, M. Ladouceur, B. Diebold, *et al.*, *Age-specific changes in left ventricular diastolic function: a velocity-encoded magnetic resonance imaging study,* European radiology **25**, 1077 (2015).

[49] A. Florian, A. Ludwig, B. Stubbe-Dräger, M. Boentert, P. Young, J. Waltenberger, S. Rösch, U. Sechtem, and A. Yilmaz, *Characteristic cardiac phenotypes are detected by cardiovascular magnetic resonance in patients with different clinical phenotypes and genotypes of mitochondrial myopathy,* Journal of Cardiovascular Magnetic Resonance **17**, 40 (2015).

[50] R. A. Weir, I. K. Tsorlalis, T. Steedman, H. J. Dargie, R. Fraser, J. J. McMurray, and J. Connell, *Aldosterone and cortisol predict medium-term left ventricular remodelling following myocardial infarction,* European journal of heart failure **13**, 1305 (2011).

[51] A. H. Ellims, H. Pfluger, M. Elsik, M. J. Butler, J. L. Hare, and A. J. Taylor, *Utility of cardiac magnetic resonance imaging, echocardiography and electrocardiography for the prediction of clinical response and long-term survival following cardiac resynchronisation therapy,* The international journal of cardiovascular imaging **29**, 1303 (2013).

[52] S. M. Adhyapak, P. G. Menon, V. R. Parachuri, K. Gadabanahalli, V. R. Bhat, V. Shetty, and D. Shetty, *Restoration of optimal left ventricular apical geometry and rotation following surgical ventricular restoration using rectangular patch plasty technique: a pilot study using cardiac magnetic resonance,* Interactive cardiovascular and thoracic surgery **19**, 398 (2014).

[53] A. A. Young and A. F. Frangi, *Computational cardiac atlases: from patient to population and back,* Experimental physiology **94**, 578 (2009).

[54] M. C. Dulce, G. H. Mostbeck, K. K. Friese, G. R. Caputo, and C. B. Higgins, *Quantification of the left ventricular volumes and function with cine mr imaging: comparison of geometric models with three-dimensional data.* Radiology **188**, 371 (1993).

[55] C. A. Miller, P. Jordan, A. Borg, R. Argyle, D. Clark, K. Pearce, and M. Schmitt, *Quantification of left ventricular indices from ssfp cine imaging: Impact of real-world variability in analysis methodology and utility of geometric modeling,* Journal of Magnetic Resonance Imaging **37**, 1213 (2013).

[56] H. Thiele, I. Paetsch, B. Schnackenburg, A. Bornstedt, O. Grebe, E. Wellnhofer, G. Schuler, E. Fleck, and E. Nagel, *Improved accuracy of quantitative assessment of left ventricular volume and ejection fraction by geometric models with steady-state free precession,* Journal of Cardiovascular Magnetic Resonance **4**, 327 (2002).

[57] J. Schulz-Menger, D. A. Bluemke, J. Bremerich, S. D. Flamm, M. A. Fogel, M. G. Friedrich, R. J. Kim, F. von Knobelsdorff-Brenkenhoff, C. M. Kramer, D. J. Pennell, *et al.*, *Standardized image interpretation and post processing in cardiovascular magnetic resonance: Society for cardiovascular magnetic resonance (scmr) board of trustees task force on standardized post processing,* Journal of Cardiovascular Magnetic Resonance **15**, 35 (2013).

[58] D. T. Ginat, M. W. Fong, D. J. Tuttle, S. K. Hobbs, and R. C. Vyas, *Cardiac imaging: Part 1, mr pulse sequences, imaging planes, and basic anatomy,* American Journal of Roentgenology **197**, 808 (2011).

[59] E. L. C. M. Matthew Brett, Michael Hanke, *Defining the dicom orientation,* (2017).

[60] P. A. Yushkevich, J. Piven, H. Cody Hazlett, R. Gimpel Smith, S. Ho, J. C. Gee, and G. Gerig, *User-guided 3D active contour segmentation of anatomical structures: Significantly improved efficiency and reliability,* Neuroimage **31**, 1116 (2006).

[61] S. Klein, M. Staring, K. Murphy, M. A. Viergever, and J. P. Pluim, *elastix: a toolbox for intensity-based medical image registration,* IEEE Transactions on Medical Imaging **29**, 196 (2010).

[62] D. P. Shamonin, E. E. Bron, B. P. Lelieveldt, M. Smits, S. Klein, and M. Staring, *Fast parallel image registration on cpu and gpu for diagnostic classification of alzheimer's disease,* Frontiers in Neuroinformatics **7**, 1 (2014).

[63] R. V. Garimella and B. K. Swartz, *Curvature estimation for unstructured triangulations of surfaces,* Los Alamos National Laboratory (2003).

[64] F. Cazals and M. Pouget, *Estimating differential quantities using polynomial fitting of osculating jets,* Computer Aided Geometric Design **22**, 121 (2005).

[65] L. Zhong, Y. Su, S.-Y. Yeo, R.-S. Tan, D. N. Ghista, and G. Kassab, *Left ventricular regional wall curvedness and wall stress in patients with ischemic dilated cardiomyopathy,* American Journal of Physiology-Heart and Circulatory Physiology **296**, H573 (2009).

[66] P. Micó, *stltools,* (2015).

[67] D.-J. Kroon, *Patch curvature,* (2014).